© 2018. Published by The Company of Biologists Ltd | Journal of Cell Science (2018) 131, jcs206920. doi:10.1242/jcs.206920

RESEARCH ARTICLE

A two-phase response of endothelial cells to hydrostatic pressure

Valeria Prystopiuk[1,2,*], Benedikt Fels[1,2], Caroline Sophie Simon[3,2], Ivan Liashkovich[1,2], Dzmitry Pasrednik[1,2], Cornelius Kronlage[1,2], Roland Wedlich-Söldner[3,2], Hans Oberleithner[1,2] and Johannes Fels[3,2,‡]

ABSTRACT

The vascular endothelium is exposed to three types of mechanical forces: blood flow-mediated shear stress, vessel diameter-dependent wall tension and hydrostatic pressure. Despite considerable variations of blood pressure during normal and pathological physiology, little is known about the acute molecular and cellular effects of hydrostatic pressure on endothelial cells. Here, we used a combination of quantitative fluorescence microscopy, atomic force microscopy and molecular perturbations to characterize the specific response of endothelial cells to application of pressure. We identified a two-phase response of endothelial cells with an initial response to acute (1 h) application of pressure (100 mmHg) followed by a different response to chronic (24 h) application. While both regimes induce cortical stiffening, the acute response is linked to Ca^{2+}-mediated myosin activation, whereas the chronic cell response is dominated by increased cortical actin density and a loss in endothelial barrier function. GsMTx-4 and amiloride inhibit the acute pressure response, which suggests that the ENaC Na^{+} channel is a key player in endothelial pressure sensing. The described two-phase pressure response may participate in the differential effects of transient changes in blood pressure and hypertension.

KEY WORDS: Endothelium, Hemodynamics, Vascular biology, High blood pressure

INTRODUCTION

In vivo, almost all tissues experience and adapt to constant mechanical stimulation. The vascular endothelium is exposed to a particularly wide variety of mechanical stresses. It must withstand constant shear stress through blood flow, vessel diameter-dependent tensile forces and blood pressure-mediated hydrostatic pressure. Each of these stimuli is essential for normal blood vessel development and function, but, if not properly controlled, they can also lead to life threatening pathological conditions. The signaling pathways of endothelial shear- and tension-sensing and their role in cardiovascular physiology have been well investigated (Davies, 2009; Hahn and Schwartz, 2009; Lehoux et al., 2006; Shimamura et al., 1999). On the systemic level, chronically increased hydrostatic pressure (i.e. hypertension), leads to cardiovascular dysfunction, atherosclerosis and organ damage. Paradoxically, although blood pressure is a major cardiovascular risk factor, little is known about the specific effect of hydrostatic pressure on endothelial cells. Nevertheless, it has been shown that chronic pressure alterations do influence cell behavior. For instance, differentiation, migration and proliferation of chondrocytes, pancreatic cells, osteoblasts and endothelial cells are dependent on their surrounding hydrostatic pressure (Acevedo et al., 1993; Elder and Athanasiou, 2009; Fels et al., 2016; Schwartz et al., 1999; Smith et al., 2004; Sumpio et al., 1994). Furthermore, cells adapt to pressurization by modulating their cytoskeletal dynamics. Endothelial cells, osteoblasts and bone marrow-derived stem cells alter the distribution, density and length of actin stress fibers in response to hydrostatic pressure (Martin et al., 2005; Müller-Marschhausen et al., 2008; Salwen et al., 1998; Thoumine et al., 1995). As actin dynamics strongly influence a wide variety of cell functions (Fels et al., 2012; Kasas et al., 2005; Oberleithner et al., 2009; Szczygiel et al., 2011), hydrostatic pressure is expected to directly affect features such as adhesion, nitric oxide release and permeability of endothelial cells (Fels et al., 2014; Glogauer et al., 1997; Jaasma et al., 2007; Matthews et al., 2006; Schnittler et al., 2014).

To date, cellular adaptations to hydrostatic pressure have been extensively characterized under long-term treatment conditions. In contrast, almost nothing is known about acute effects of pressure variations on endothelial cells. This is surprising, as the vasculature is frequently exposed to short-term pressure variations. For instance, physical exercise transiently increases blood pressure, for a duration of several minutes to a few hours, and is linked to beneficial effects on the cardiovascular system. In contrast, hypertension is characterized by a long-term increase in pressure (days to weeks) and is classified as a key cardiovascular risk factor. Likewise vascular pressure varies significantly during daily routine without any direct negative effect on the vasculature. To identify potential differences in acute versus chronic pressure responses, a detailed analysis of endothelial actin-myosin dynamics and their physiological consequences as a function of the duration of physiological pressure exposure is necessary. Furthermore, it remains elusive how cells can sense hydrostatic pressure in the first place, as the molecular nature of a potential pressure sensor is still unknown. There is some evidence for Ca^{2+}, purinergic signaling, RhoA, Rac1 and NF-KB being involved in the adaption to changes in ambient (the background; ∼760 mmHg, 101 kPa) pressure (Gardinier et al., 2014; Mandal et al., 2010; Sappington et al., 2009; Zhao et al., 2015). However, these messenger ions/signaling molecules are likely downstream targets of the actual pressure sensor. Even intracellular structures are predicted to act as sensors for mechanical stress. For instance, non-muscle myosin II can sense mechanical stress and adapt its function (Kim et al., 2015; Luo et al., 2012). However, such motor proteins usually react to a non-isotropically applied stress with a distinct spatial localization (e.g. tension or shear stress), while, in contrast, blood pressure acts isotropically on whole endothelial cells.

[1]Institute of Physiology II, University of Münster, Robert-Koch-Str. 27b, 48149 Münster, Germany. [2]Institute of Cell Dynamics and Imaging, University of Münster, Von-Esmarch-Str. 56, 48149 Münster, Germany. [3]Cells-In-Motion Cluster of Excellence (EXC1003-CiM), University of Münster, 48149, Münster, Germany. *Present address: Institute of Life Sciences, Université Catholique de Louvain, Croix du Sud, 4-5, bte L7.07.06, Louvain-la-Neuve B-1348, Belgium.

‡Author for correspondence (felsj@uni-muenster.de)

V.P., 0000-0001-9316-8635; I.L., 0000-0002-0025-6124; C.K., 0000-0002-3681-1943; J.F., 0000-0001-7731-3265

Received 31 May 2017; Accepted 10 May 2018

Journal of Cell Science (2018) 131, jcs206920. doi:10.1242/jcs.206920

Mechanosensitive ion channels (MSCs) are the most promising candidates in the search for pressure sensors, as these channels also react to other mechanical stimuli, such as shear and tensile stress (Nilius and Droogmans, 2001). Ca^{2+} and Na^{+} channels have been postulated to be involved in pressure-mediated signaling (Fels et al., 2016; Guo et al., 2016; Liu and Montell, 2015; Nilius and Droogmans, 2001; O'Hagan et al., 2005).

Here, we show that endothelial cells exhibit a two-phase response to elevated hydrostatic pressure. An acute increase in pressure causes rapid, Ca^{2+}-dependent activation of myosin. This results in increased 'line' tension within the cortical acto-myosin web and hence stiffening of the cell cortex. This effect is rapidly reversible once cells are returned to ambient pressure. Upon chronic or long-term exposure to increased pressure, endothelial cells show a stiffer cell cortex through increased polymerization of actin and formation of a denser actin cortex. This effect is not immediately reversible. In addition, the chronic response is accompanied by a breakdown of the endothelial barrier function, which is not affected during the acute response. Finally, we performed inhibitor studies that identified amiloride- and GsMTx-4-sensitive ion channels as key players in endothelial pressure sensing.

RESULTS

Actin polymerizes in response to chronic pressure

To facilitate controlled exposure of cells to elevated pressure we constructed a cell culture-compatible chamber, which allows cultivation of cells at elevated hydrostatic pressure for extended periods (for details, see Materials and Methods section and Fig. 1).

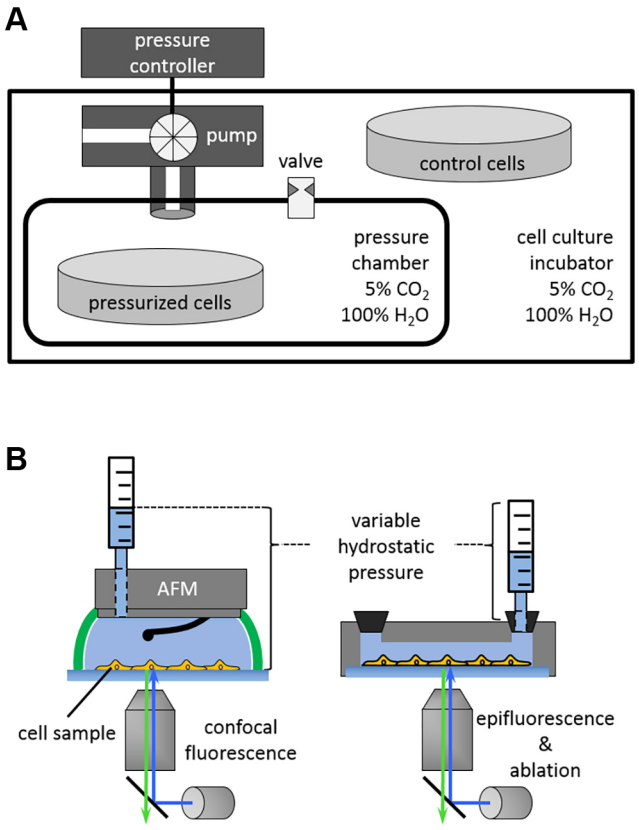

Fig. 1. Pressure chamber set up used in the current study. (A) Pressure chamber used for chronic pressure incubation. (B) Live-cell imaging pressure chambers facilitating AFM, fluorescence microscopy and laser ablation, as indicated. See the Materials and Methods for more details.

A change in blood pressure of 100 mmHg is characteristic for severe hypertension but can also be reached transiently during physical exercise. Therefore, we have chosen a pressure change of ΔP=100 mmHg (i.e. 13 kPa, hereafter referred as 100 mmHg) as our biological model system. To analyze differential effects of short-term and long-term pressure application, bovine aortic endothelial cells (GM7373) were exposed to a 100 mmHg pressure increase for either 1 h (acute) or 24 h (chronic), and subsequently the global level cellular actin polymerization was quantified. Western blot analysis showed an increase of the F-actin:G-actin ratio that depended on the duration of pressure exposure (Fig. 2A). While we only found a mild increase after 1 h exposure to 100 mmHg (Fig. 2B, 1.8±0.4 fold, P=0.05, mean±s.e.m.), pressurization for 24 h led to a strong increase of 4.21±1.11 fold (P=0.04) compared to control conditions (Fig. 2A). This increase in actin polymerization upon chronic pressure exposure nicely confirms previous results in various cell types (Martin et al., 2005; Müller-Marschhausen et al., 2008; Salwen et al., 1998; Thoumine et al., 1995). Furthermore, we quantified changes in tubulin expression (Fig. 2B; Fig. S2B), but could not detect any pressure-dependent alterations. While testing for acetylated tubulin, which can be used as an indicator for increased tubulin stability (Portran et al., 2017), only a mild and non-significant increase in tubulin acetylation could be found after 24 h at 100 mmHg (Fig. 2B; Fig. S2B). Similarly, intermediate filaments seem to be unaffected by pressure, as again only a mild increase for vimentin expression was detected during chronic pressure application (Fig. 2B, Fig. S2B). Hence, it can be concluded that actin, but not intermediate filaments or microtubules, is affected by hydrostatic pressure.

It is important to note that quantification of overall cellular actin polymerization does not indicate specific changes in any particular actin structure or compartment. As organization and dynamics of the cortical acto-myosin web is critical for function of endothelial cells (Fels et al., 2014; Szczygiel et al., 2011), we next wanted to take a closer look at the actual actin distribution. We fixed cells directly after pressure exposure and stained filamentous actin with TRITC–phalloidin. By using spinning disk microscopy, we then quantified actin fluorescence at the apical and basal cortex areas (i.e. the most apical focal plane as well as the basal focal plane), respectively. At ambient pressure, GM7373 cells exhibit characteristic actin bundles at the basal cell periphery and a dense apical actin meshwork (Fig. 2C,E; Kronlage et al., 2015). Upon acute pressure application, neither density nor organization of basal and apical actin was altered (Fig. 2C,D). In contrast, after 24 h exposure to elevated pressure, the apical F-actin intensity increased by 1.65±0.05 fold (P<0.01, Fig. 2D) and the basal actin intensity was increased by 1.4±0.07 fold compared to control (P<0.01, Fig. 2F). In addition, we observed increased lamellipodia formation, which is indicative of a reduced stability in cell–cell contacts (Fig. 2E). To characterize actin dynamics in more detail, we further stained for actin cross linkers and cofilin family proteins, and checked for differences in their expression level and localization. We could neither detect any pressure-dependent alteration in intensity nor in its distribution for α-actinin-1 (Fig. S2C). In contrast, the network forming actin cross-linker α-filamin was increased in response to acute (P<0.01) as well as chronic (P<0.01) pressure application (Fig. S2D). Interestingly, we found that cofilin activity (ambient versus 1 h, P<0.01; ambient versus 24 h, P<0.01), but not expression, was inhibited upon pressure application (Fig. S2E). Our results confirm previous findings that actin polymerization in various cell types is increased upon long-term increase of hydrostatic pressure (Martin et al., 2005; Müller-Marschhausen et al., 2008; Salwen et al., 1998; Thoumine et al., 1995).

Journal of Cell Science (2018) 131, jcs206920. doi:10.1242/jcs.206920

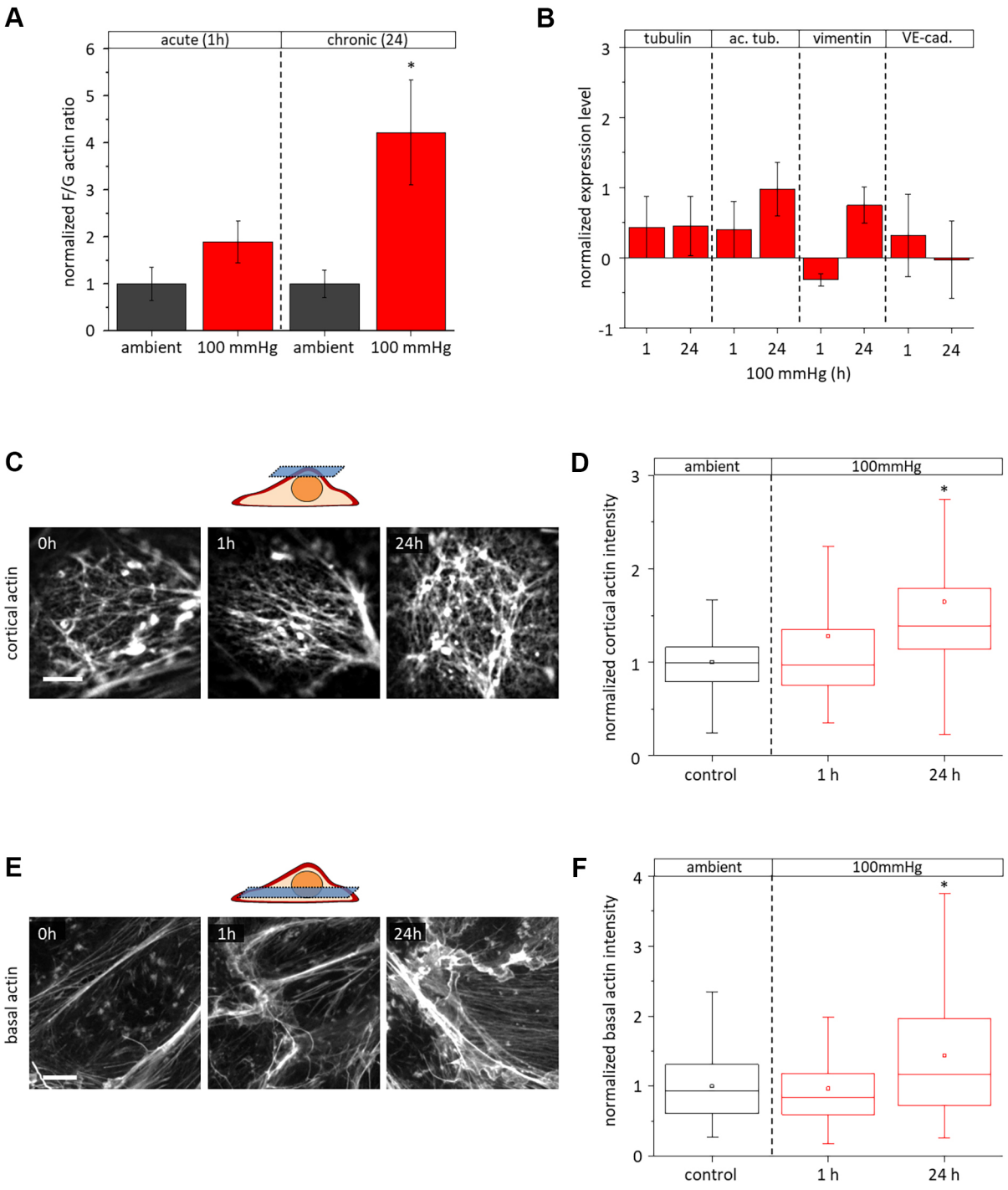

Fig. 2. Pressure-dependent actin organization and pressure-dependent actin polymerization. (A) Western blot quantification of F- and G-actin, used to determine the F-actin:G-actin (F/G actin) ratio for GM7373 cells in the indicated conditions. G-actin samples were diluted 10 fold. NUP62 appears in F-actin fractions, as a control of proper separation (n=5). A representative blot is shown in Fig. S2A. (B) Quantification of the levels of tubulin, acetylated tubulin (ac. tub.), vimentin and VE-cadherin (n=4) for GM7373 cells in the indicated conditions. A representative blot is shown in Fig. S2B. (C,D) Effects of hydrostatic pressure on apical F-actin organization in GM7373 cells. Immunofluorescence images of TRITC–phalloidin are shown after pressure application (100 mmHg) for 1 h and 24 h. Actin intensity is increased after 24 h of pressure application (n>117). Scale bar: 10 µm. (E,F) Basal F-actin organization in response to 1 h or 24 h pressure application (100 mmHg), showing increased F-actin abundance in chronic response to pressure (n>209). Scale bar: 5 µm. *P<0.05 compared to respective ambient control.

Endothelial cells stiffen in response to acute hydrostatic pressure

Cortical actin dynamics influence the mechanical properties of cells, which are in turn instrumental for proper endothelial function. As we and others have shown before, stiffness of the apical endothelial cortex correlates directly with endothelial function. Nitric oxide release (Fels et al., 2014; Szczygiel et al., 2011), inflammatory response (Lee et al., 2011) as well as barrier function and the route of leukocyte diapedesis (Martinelli et al., 2014) correlate to endothelial nanomechanics. Owing to the high correlation of

Journal of Cell Science (2018) 131, jcs206920. doi:10.1242/jcs.206920

cortical stiffening to endothelial function, a 'stiff endothelial cell syndrome' has been postulated (Lang, 2011). We therefore analyzed the mechanical properties of the apical endothelial cortex during acute and chronic pressure response by performing atomic force microscopy (AFM). To prevent any potential recovery from pressure treatments, cells were initially fixed before measurements. Importantly, it has been previously shown that the mechanical properties of fixed cells correlate well with those of living cells. Although fixed cells are generally stiffer than living cells, the mechanics of fixed control cells differ to those of fixed treated cells (Codan et al., 2013; Grimm et al., 2014; Targosz-Korecka et al., 2015). Surprisingly, we found that, in contrast to the unaltered actin levels, cortical stiffness of pressurized cells had already increased by 1.36±0.03 fold after an acute elevation of pressure for 1 h (P<0.01, Fig. 3A). This acute stiffening was fully reversible, as cortical stiffness rapidly decreased to 0.97±0.07 of the original value upon pressure reduction to ambient level for 1 h (Fig. 3A). Endothelial cells that were pressurized for 24 h exhibited significantly increased cortical stiffness (1.47±0.02-fold increase, P<0.01; Fig. 3A). This is consistent with our quantified actin staining (Fig. 2C–F), as well as previous reports linking increased cortical actin density to higher cortical stiffness (Laudadio et al., 2005). In contrast to the acute treatment, the pressure-induced stiffening was irreversible after exposure to chronically increased pressure. Stiffness remained 1.43±0.05-fold increased after 1 h ambient recovery (P=0.01, Fig. 3A).

To validate our results and to exclude potential fixation-induced artifacts, we designed a second pressure chamber to allow us to perform live-cell AFM at adjustable hydrostatic pressure. By using this pressure chamber, we were able to directly follow the mechanical properties of cells during pressure application. Cells were initially recorded at ambient pressure for 30 min to obtain their baseline stiffness. During subsequent exposure to increased hydrostatic pressure for 60 min, the cell cortex rapidly stiffened within a few minutes (by 1.46±0.17 fold, P=0.02) and remained elevated during continuous pressure application (Fig. 3B,C). This increase in cortical stiffness was fully reversible, and values returned to baseline values within 30 min of pressure relief (Fig. 3B). To investigate the acute effect on cortical stiffening in more detail, we measured cortical stiffening at various pressure loads (Fig. 3C). We found no detectable stiffening at loads of 60 mmHg (1.11±0.1 fold, P=0.73) and an intermediate increase of cell stiffness at 80 mmHg cells (1.21±0.07 fold, P=0.01). We further validated the identified acute pressure effect on primary human umbilical endothelial cells (HUVECs) as well as on the human endothelial cell line EA.hy926 (mock siRNA transfected; see below). Similar to what we observed with the GM7373 cells, HUVECs and EAhy926 cells stiffened by 1.51±0.1 (P<0.01) and 1.58±0.06 fold (P<0.01), respectively, upon pressure elevation of 100 mmHg for 1 h (Fig. 3C). These results indicate that cortical stiffening in response to acute exposure to hydrostatic pressure is likely a general property of vasculature endothelial cells.

In summary, we found that endothelial cells exhibit differential mechanical adaptations to acute pressurization compared to those seen for chronic pressurization. While extended periods of pressure application stiffen the cell cortex due to an overall increase in actin filament levels and density, acute pressurization leads to cortical stiffening that is independent of F-actin polymerization.

Cortical myosin is activated in the acute pressure response

In addition to actin polymerization, cortical stiffness can also be regulated by changes in actin filament cross linking or acto-myosin contractility (Martens and Radmacher, 2008; Schillers et al., 2010). To characterize a potential contribution of motor proteins to the pressure-response in endothelia, we first imaged myosin heavy chain A (MHCA; also known as MYH9) expression in GM7373 cells. As shown in Fig. 4A,B, we already found a significant increase in MHCA expression during the early response to 100 mmHg. Basal and apical signal intensities increased within 1 h at 100 mmHg (1.43±0.06, P<0.01, and 1.39±0.1, P<0.01 fold of ambient control, respectively). The response to chronic pressure application was even stronger, both in basal (1.83±0.1, P<0.01) and apical cortex (1.79±0.14, P<0.01). To assess myosin activity, we further quantified the level of myosin light chain (MLC; also known as MYL2) and activated phosphorylated MLC (pMLC) by western blot and immunofluorescence. Interestingly, neither the total

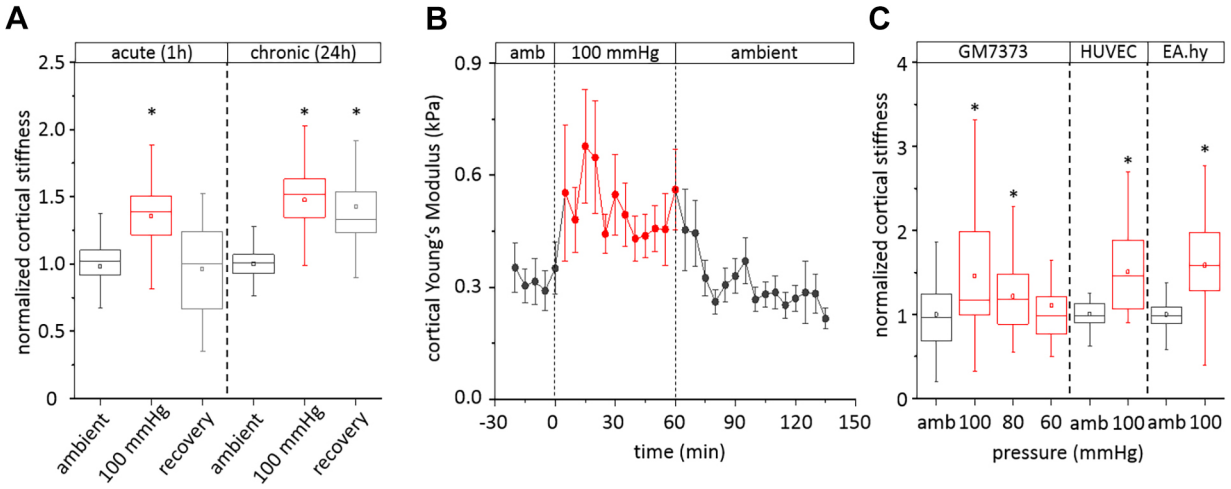

Fig. 3. Pressure-induced changes in cortical cell stiffness. Measurements of cortical stiffness via AFM after different regimes of hydrostatic pressure increase. (A) Comparison of cortical stiffness in acutely (1 h) and chronically (24 h) pressurized cells (n>92) and after subsequent reversion to ambient pressure for 1 h (n>18). Experiments were performed with GM7373 cells that were fixed after pressure application. (B) Live-cell stiffness measurement of cortical stiffness during 1 h pressure application in GM7373 cells (100 mmHg) (n=19). (C) Quantification of pressure-induced stiffening in live cells in response to different acute (1 h) pressure, showing an increases for GM7373 (n>27), HUVECs (n=21) and EAhy.926 mock RNAi cells (n=67). The results for EAhy.926 mock RNAi cells are also shown in Fig 6. *P<0.05 compared to respective ambient control.

Journal of Cell Science (2018) 131, jcs206920. doi:10.1242/jcs.206920

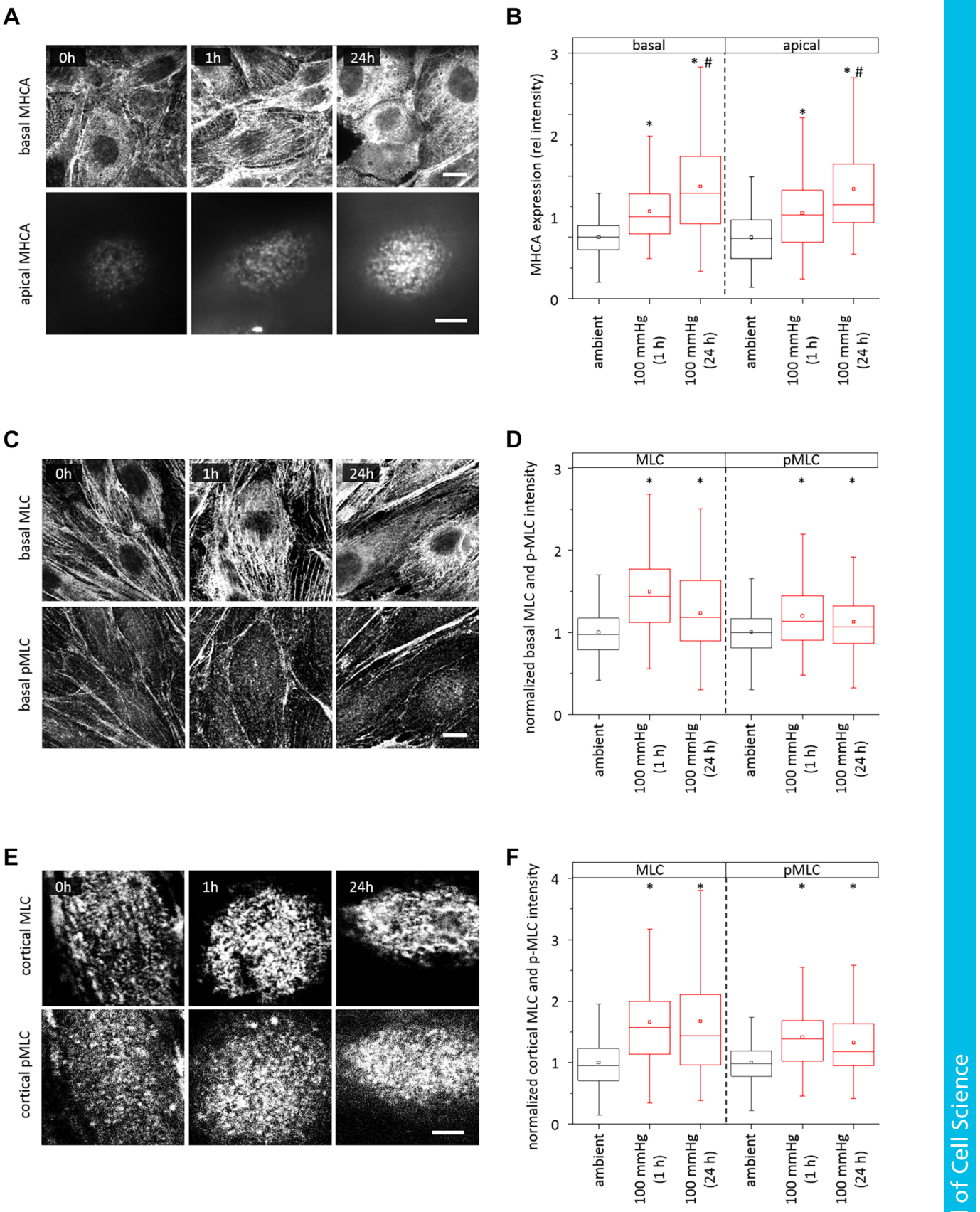

Fig. 4. Pressure-dependent expression and activation of non-muscle myosin. (A,B) Basal and apical immunofluorescence images (A) of non-muscle myosin II A in GM7373 cells and quantification (B) of respective fluorescence intensities ($n \geq 62$). (C,D) Immunofluorescence labeling (C) and quantification (D) of basal MLC and pMLC fluorescence intensities ($n > 104$). (E,F) Immunofluorescence labeling (E) and quantification (F) of apical MLC and p-MLC ($n > 125$). Scale bars: 10 µm (basal); 5 µm (apical). $^{*}P<0.05$ compared to respective ambient control; $^{\#}P<0.05$ compared to 1 h 100 mmHg.

Journal of Cell Science (2018) 131, jcs206920. doi:10.1242/jcs.206920

MLC expression nor its overall phosphorylation state changed significantly as determined by western blot analysis in response to the 100 mmHg pressure increase (Fig. S3A,B).

However, as the function of myosin is largely dependent on its cortical distribution, we also quantified the levels of MLC and pMLC specifically at the basal and apical surfaces of cells. At the basal side, we found a significant increase of MLC levels and activity after acute exposure to 100 mmHg (MLC, 1.49±0.04, P<0.01; pMLC, 1.2±0.03, P<0.01; Fig. 4D,F), and this change was largely retained after chronic pressurization (MLC, 1.24±0.05, P<0.01; pMLC, 1.13±0.03, P<0.01; Fig. 4D,F). This pressure-dependent effect on MLC abundance and activation was even more pronounced at the apical cell cortex, as there the levels increased to 1.66±0.06 (P<0.01) and 1.41±0.03 (P<0.01) during acute pressure exposure, as well as to 1.67±0.08 (P<0.01) and 1.32±0.04 (P=0.04) for MLC and pMLC during chronic pressure application, respectively (Fig. 4D,F). Our results indicate that myosin activation plays a role in the acute response of endothelial cells to changes in pressure.

Pressure-dependent myosin activation increases line tension

As the above results suggest that non-muscle myosin II activity is increased during acute exposure of cells to hydrostatic pressure, we set out to directly observe and quantify myosin-mediated tension in the apical acto-myosin web. To this end, we first measured the cortical Young's modulus of pressurized endothelial cells in the absence or presence of 5 µM of the specific myosin II inhibitor blebbistatin. Even at ambient pressure, the inhibitor induced softening of the apical cortex [$YM_{(wt)}$=0.3±0.02 kPa, $YM_{(bleb)}$=0.2±0.01 kPa; Fig. 5A]. More importantly, the observed pressure-dependent stiffening (0.55±0.06 kPa after 1 h at 100 mmHg) was completely reversed upon blebbistatin administration (0.19±0.02 kPa, Fig. 5A). To verify whether myosin indeed increased contractile tension within the cortical acto-myosin web, we performed laser ablation experiments on cortical acto-myosin filaments (using GM7373 cells stably expressing MLCb–GFP; MLCb is also known as MYL12A). A pulsed UV laser was used to cut individual apical acto-myosin filaments (Fig. 5B). At ambient pressure, cortical filaments exhibit an average retraction velocity of 478±18 nm/s (Fig. 5C). Upon an acute increase in pressure, filament retraction velocity increased by 30% to 631.6±24.5 nm/s (P<0.01). This elevation of 'line' tension was again reversible (to 521.5±21.1 nm/s) after 1 h recovery at ambient pressure (Fig. 5C; Movie 1). Interestingly, the retraction velocities of cut basal stress fibers were even faster, but did not noticeably change upon the increase in pressure (ambient, 841.2±53.8 nm/s; 1 h 100 mmHg, 811.0±40.3 nm/s, P=0.06, Fig. 5D). However, the latter numbers have to be taken with a note of caution. We found that stress fiber ablation often induced whole-cell rupture, likely due to simultaneous injury of the plasma membrane, potentially interfering with our quantification.

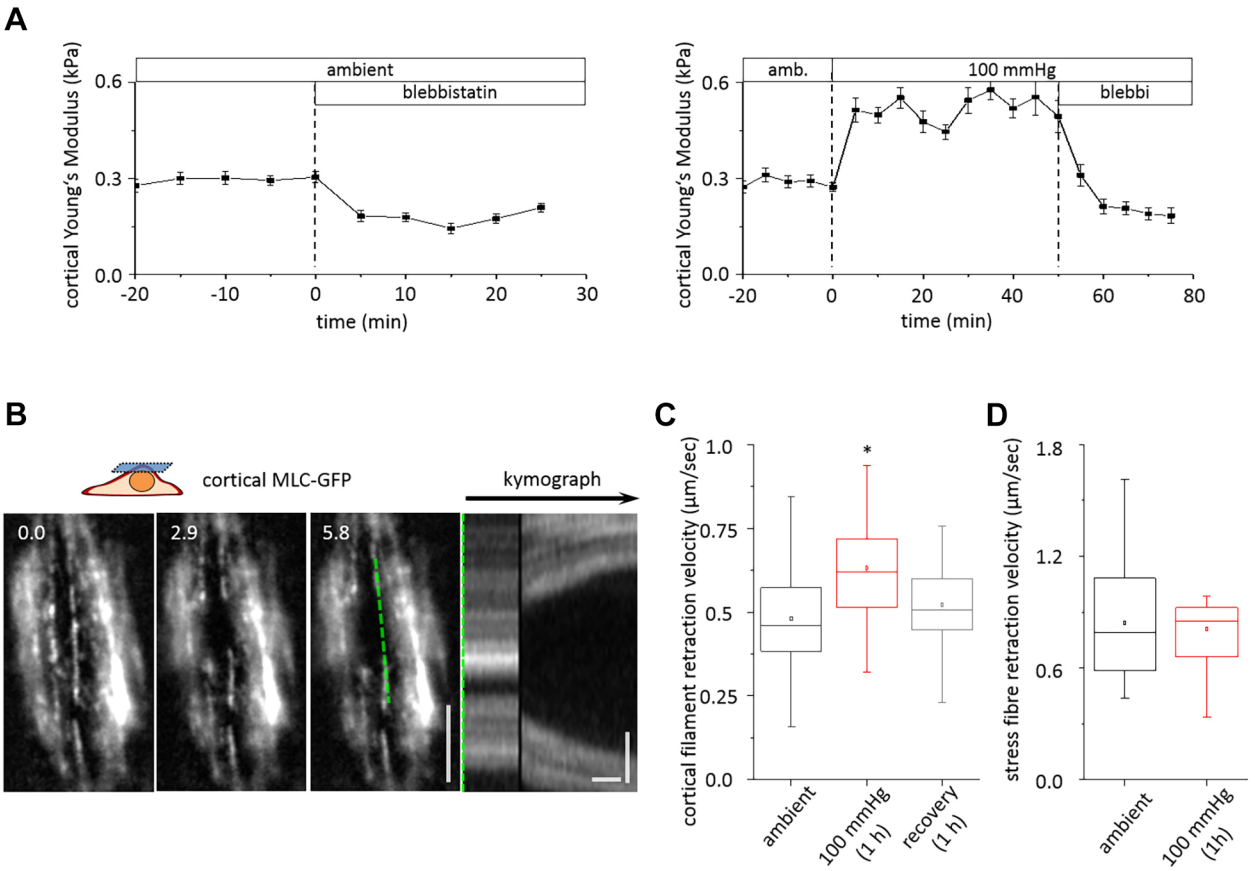

Fig. 5. The effect of pressure on myosin-mediated line tension. (A) Effect of treatment with 5 µM blebbistatin on stiffness of GM7373 cells (n=54) at ambient pressure and 100 mmHg. (B) Example illustrating ablation of single cortical acto-myosin filaments. The kymograph (right) is shown for the trajectory along the dotted green line. Time is in seconds. Scale bars: 1 s (horizontal), 5 µm (vertical). (C) Retraction velocities of cortical acto-myosin filaments after acute exposure to increased hydrostatic pressure and after recovery at ambient pressure (n≥61). (D) Retraction velocities of basal stress fibers after acute exposure to increased hydrostatic pressure (n≥27). *P<0.05 compared to respective ambient control.

Journal of Cell Science (2018) 131, jcs206920. doi:10.1242/jcs.206920

In summary, we found that endothelial cells react to acute pressure application via cortical recruitment and activation of type II myosin proteins.

Pressure-induced Ca^{2+} entry is mediated by mechanosensitive cation channels

We next wanted to investigate how endothelial cells can sense and transmit changes in hydrostatic pressure to regulate myosin activity. Likely candidates for endothelial pressure sensors are MSCs and, in particular, Ca^{2+} channels, considering the central role of Ca^{2+} in myosin activation and acto-myosin contractility. Hence, we set out to characterize endothelial Ca^{2+} signaling in response to acute changes in pressure load. To quantify changes in intracellular Ca^{2+} concentration, endothelial cells were loaded with the fluorescent Ca^{2+} marker Fluoforte and imaged during pressure exposure. We measured changes in resting Ca^{2+} levels as well as the frequency of Ca^{2+} oscillations. While resting Ca^{2+} remained stable at ambient pressure (Fig. 6A), its levels immediately increased upon pressure exposure, finally reaching a plateau after 60 min (Fig. 6A,B; Movie 2). In addition, we detected distinct changes in the pattern of intracellular Ca^{2+} oscillations (Fig. S4; Movie 3). At ambient pressure, about one third of all endothelial cells exhibited spontaneous Ca^{2+} oscillations (i.e. two or more Ca^{2+} sparks within a 10 min interval). At ambient pressure, Ca^{2+} sparks reached a 1.4±0.06 fold peak intensity (Fig. 6C) with a mean duration of 49.2±2.4 s (Fig. 6D) and an average oscillation frequency of 0.32±0.01 min^{-1} (Fig. 6E). An acute elevation of hydrostatic pressure by 100 mmHg did not influence peak intensity (1.3±0.02, P=0.41) or duration (47.2±1.5 s, P=0.74) of Ca^{2+} sparks (Fig. 6C,D). Interestingly, the fraction of cells showing Ca^{2+} oscillation increased to 51%, and the oscillation frequency increased at the single-cell level directly upon pressure elevation to an average 0.43±0.03 min^{-1} (Fig. 6E, P<0.01). Hence, a rise in hydrostatic pressure increases both basal Ca^{2+} levels and the frequency of Ca^{2+} oscillations in cells.

Ca^{2+} and Na^{+} channels have been postulated to be involved in pressure-mediated signaling (Liu and Montell, 2015; Nilius and Droogmans, 2001; O'Hagan et al., 2005). To test the role of these channel types in endothelial pressure sensing, we quantified pressure-dependent Ca^{2+} influx and line tension in the presence of specific MSC blockers. GsMTx-4 is an inhibitor of mechanosensitive Ca^{2+} channels, including TRPC1, TRPC6 and stretch-activated ion channels (Bowman et al., 2007).

Incubation of GM7373 cells with 5 µM GsMTx-4 nearly abolished the pressure-dependent increase in baseline Ca^{2+} (Fig. 6A,B) and Ca^{2+} oscillation frequency (Fig. 6E, P=0.46). The inhibitor had no effect on line tension at ambient pressure (503±30 nm/s), but dampened the pressure-dependent increase in retraction velocities down to 525±21 nm/s (P=0.21, Fig. 6F). The DEG/ENaC family is another group of putative MSCs that have been proposed to play a role in pressure sensing (Tavernarakis and Driscoll, 2001), and can be inhibited by the drug amiloride. Surprisingly, although at 1 µM amiloride is reported to specifically affect the ENaC, amiloride inhibited the pressure-induced increase in Ca^{2+} levels (Fig. 6A,B) and oscillations (P=0.78, Fig. 6E). Furthermore, the inhibitor completely abolished the pressure-dependent elevation in retraction velocity (450.8±15 nm/s, P=0.13), whereas it had no measurable effect at ambient pressure (481.6±13 nm/s, Fig. 6F). In line with these findings, we observed a complete inhibition of pressure-mediated cortical stiffening upon treatment with 1 µM benzamil, an even more specific inhibitor of ENaC (Fig. 6G). However, as these inhibitors still might exhibit some side effects, we included the previously described EAhy926 ENaC knockdown cell line (RNAi) in our study (Jeggle et al., 2013). EAhy926 cells transfected with mock siRNA showed, as described above (Fig. 6H), an increase in cortical stiffness upon pressure application. ENaC-knockdown cells (siRNA against SCNN1A) showed a strongly reduced stiffening reaction to pressure elevation (1.16±0.04, P=0.11), which validates our experiments using amiloride and benzamil.

In summary, our results indicate that an acute increase in hydrostatic pressure leads to an increase in Ca^{2+} influx via mechanosensitive cation channels and that Ca^{2+}, in turn, activates myosin and increases the contractile strength of the cell cortex.

Pressure influences endothelial permeability

To test a potential effect of elevated pressure on endothelial barrier function, we analyzed the function of VE-cadherin (also known as CDH5) in endothelial cells. In western blot analysis, we could not detect any direct change in VE-cadherin expression upon pressure stimulation (Fig. S2A). While hardly any change in VE-cadherin localization was visible during acute pressure application, chronic exposure to high pressure was associated with wider and discontinuous cell–cell junctions (Fig. 7A). We calculated the area:contour length ratio of the junctional protein to quantitatively assess changes in the VE-cadherin distribution. We found a opposite effect of acute and chronic pressure on the area:contour length ratio. While acute pressure seemed to induce a concentration of VE-cadherin directly at the cell–cell contacts, the signal appeared to be discontinuous during chronic pressure application, resulting in an increased ratio (1 h versus 24 h, P=0.01; Fig. 7B). A similar effect has been described previously by others (Ohashi et al., 2007). As disassembly of cell–cell junctions, might result in an increase in endothelial permeability, we measured the transendothelial electrical resistance (TEER) of GM7373 cells after pressure application. TEER measurements showed that endothelial resistance was unchanged upon exposure to acute pressure (+2.5%, P=0.52) but was strongly reduced by 19.2% (P=0.05) during long-term pressure adaptation (Fig. 7C). As it has been shown before that increased contractility is accompanied by integrin activation and focal adhesion maturation (Vicente-Manzanares et al., 2009), we furthermore tested whether pressure affects the endothelial–matrix interaction by staining for activated integrin β1. However, we could not observe any change in the distribution or intensity in integrin β1 activation in response to pressure (Fig. S5A).

To finally validate a physiological significance of the described two-phase response of endothelial cells to changes in hydrostatic pressure, we tested for a leukocyte transmigration (transendothelial migration, TEM) dependence on pressure. We tested both unstimulated and TNFα-stimulated endothelial cells and exposed the cells to ambient pressure, or 1 h or 24 h at 100 mmHg. Neutrophils were added to the cells for a total duration of 1 h (the final hour of incubation). As expected, TNFα stimulation of endothelial cells resulted in an inflamed phenotype provoking significant increased neutrophil transmigration (Fig. 7D). Interestingly, acute pressure application did not affect TEM through unstimulated endothelia (P=0.39), while migration rates in the TNFα group stayed elevated. After 24 h of pressure application, however, there was a strong increase in TEM even through unstimulated endothelium (P=0.02, Fig. 7D).

Taken together, we have shown that endothelial cells have a two-phase response to hydrostatic pressure. During acute pressure exposure, motor proteins are activated via an ENaC-dependent mechanism resulting in an increase in intracellular Ca^{2+}.

Journal of Cell Science (2018) 131, jcs206920. doi:10.1242/jcs.206920

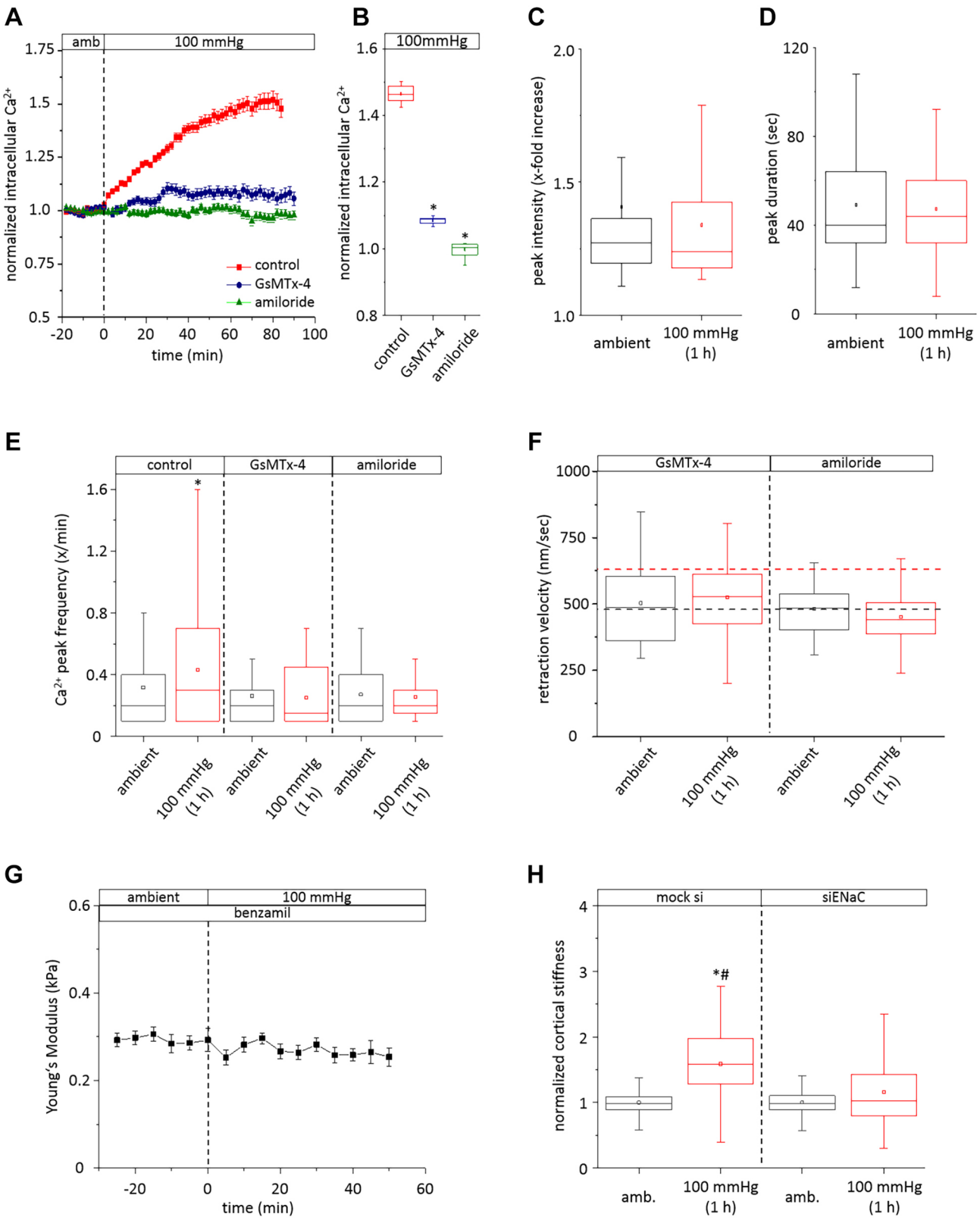

Fig. 6. The effect of pressure on Ca^{2+} signaling. (A,B) Quantifications of baseline $[Ca^{2+}]_i$ in GM7373 cells reveals a pressure-dependent increase in Ca^{2+} (red, n=131) that was blocked by treatment with GsMTx-4 (blue, n=56) and amiloride (green, n=159). (C,D) Neither peak intensity (C) nor peak duration (D) of Ca^{2+} oscillations were influenced by pressure (n=110). (E) An oscillation frequency quantification highlights the increased Ca^{2+} spark frequency upon pressure application (n>162). This effect is again inhibited by the MSC blockers GsMTx-4 (5 µM, blue, n=108) and amiloride (green, 1 µM, n=65). (F) The pressure-dependent increase in line tension was blocked by GsMTx-4 (n>32) or amiloride (n=50) treatment. Black and red horizontal dashed lines indicate the mean velocity of untreated cells at ambient and 1 h 100 mmHg pressure, respectively (see Fig. 5C). (G) The cortical Young's modulus of GM7373 cells+1 µM benzamil is unaffected by acute pressure application (n=33). (H) siENaC EA.hy926 cells show reduced cortical stiffening in response to 1 h 100 mmH exposure. Data for mock siRNA EA.hy926 cells are reproduced from Fig. 3C (n≥67). *P<0.05 compared to respective ambient control; $^{\#}P$<0.05 compared to 24 h 100 mmHg.

Journal of Cell Science (2018) 131, jcs206920. doi:10.1242/jcs.206920

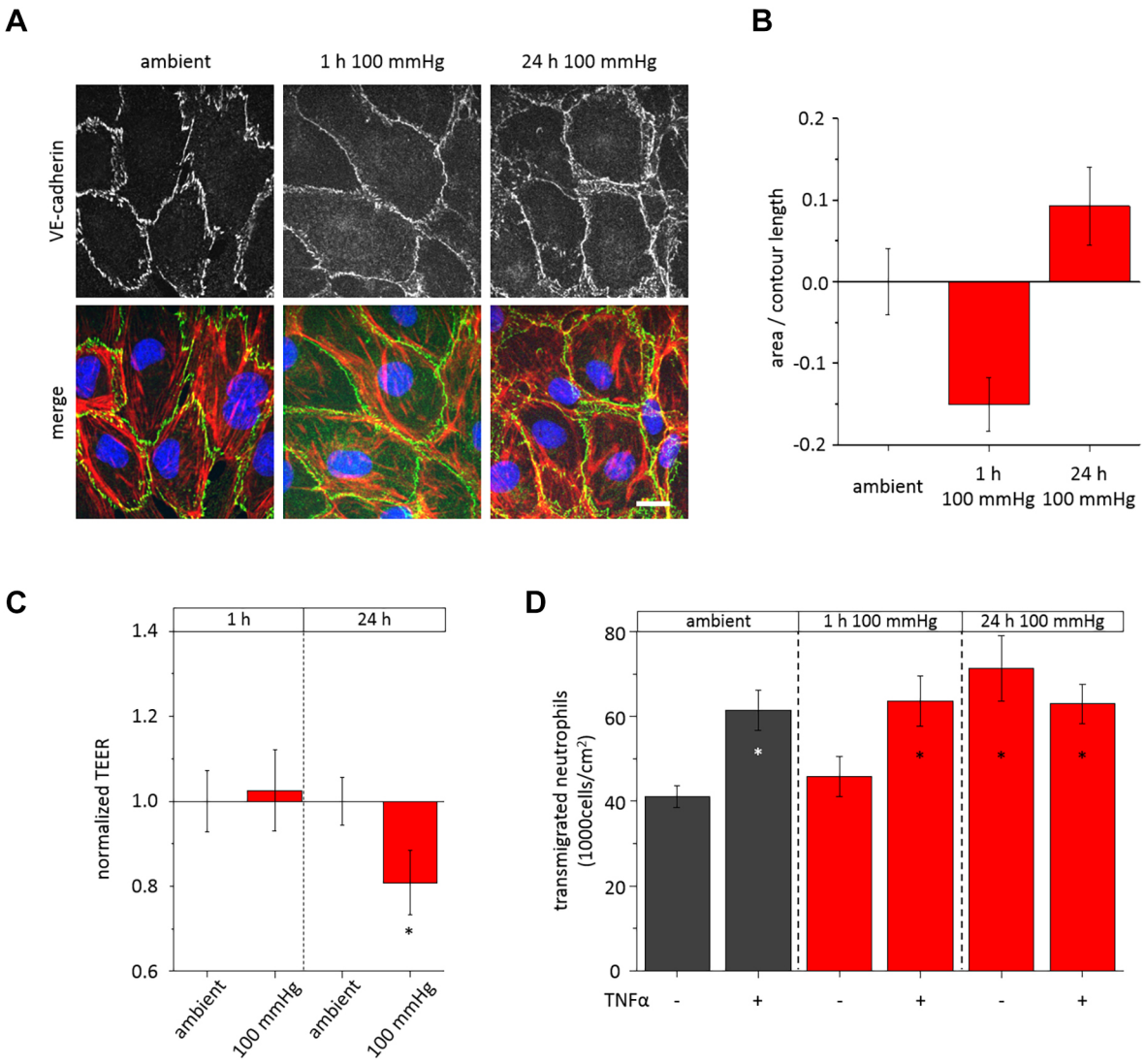

Fig. 7. Pressure-dependent endothelial permeability. (A) VE-cadherin staining of pressurized GM7373 cells. Long-term pressure exposure induces a discontinuous VE-cadherin pattern. Scale bar: 10 µm. (B) A relative change in the area:contour length ratio indicates a barrier disruption upon chronic pressure incubation ($n \geq 15$). (C) TEER measurements were used to quantify the endothelial permeability in response to pressure application, validating the finding of increased permeability as long-term response to pressure ($n=14$). (D) Quantification of Hoxb8 neutrophil transmigration (TEM) through a bEnd5 monolayer, which is increased after TNFα stimulation. While acute pressure application had no impact on TEM it is increased in the response to chronic pressure. ($n \geq 11$). *$P<0.05$ compared to respective ambient control.

A long-term increase in pressure results in actin polymerization and a loss in the endothelial barrier function.

DISCUSSION

It is well accepted that bone- and cartilage-derived cells are able to sense and react to distinct hydrostatic loads. Although blood pressure is the first clinical parameter used to give information on the physiological status of the vascular system (Ezzati et al., 2002), surprisingly little is known of the cell biological response of endothelial cells to pressure exposure. What is known is that prolonged pressure application induces remodeling of the actin cytoskeleton, which in turn links to endothelial nitric oxide release and barrier function (Fels et al., 2012; Schnittler et al., 2014; Szczygiel et al., 2011). However, (arterial) endothelial cells are frequently exposed to transient pressure alterations. Many of these variations include significant increases in hydrostatic pressure (e.g. daily routine, physical exercise). Those short-term changes are usually not associated with pathological consequences, but, by contrast, often have beneficial effects for the vascular system. As nothing is known about the short-term effect of pressure on the endothelial cytoskeleton, we set out to characterize the early steps in endothelial pressure sensing and adaptation.

Our results suggest that there is a two-phase response of endothelial cells to increased hydrostatic pressure (Fig. 8). Upon an acute elevation in pressure, intracellular Ca^{2+} levels rise and the frequency of Ca^{2+} oscillations increase. From the experiments with the MSC blockers GsMTx-4 and amiloride/benzamil, it is evident that MSCs mediate this increase in $[Ca^{2+}]_i$ and therefore potentially act as endothelial pressure sensors (Fig. 8). The exact nature of the pressure-sensing element, however, remains elusive. One might speculate that the Ca^{2+}-permeable channels of the GsMTx-4-sensitive transient receptor potential (TRP) superfamily represent the actual pressure sensor. However, the inhibitory effect of amiloride/benzamil, as well as the experiments using the ENaC-knockdown cells, indicate that TRP channels may not be the primary pressure sensor but are indirectly linked to an

Journal of Cell Science (2018) 131, jcs206920. doi:10.1242/jcs.206920

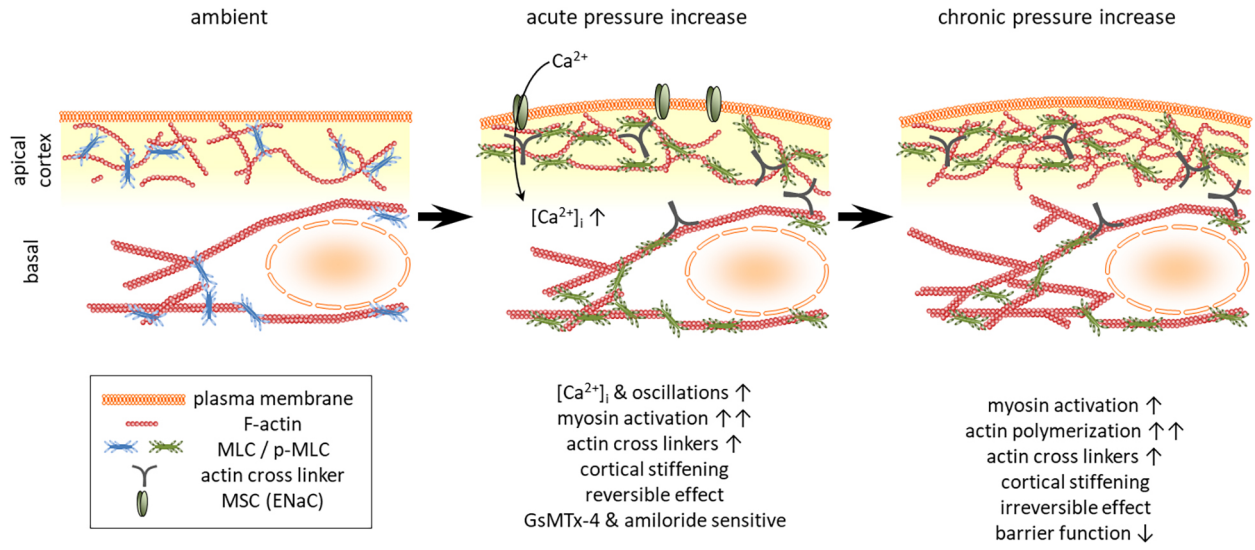

Fig. 8. Model of acute and chronic effects of hydrostatic pressure on endothelial cells. An acute pressure increase for 1 h causes Ca^{2+} entry via MSCs and subsequent cortical stiffening due to increased myosin activation. Actin polymerization is not altered in the acute response. Chronic pressure incubation (24 h) leads to cortical actin polymerization. At this stage, endothelial barrier function is decreased and neutrophil transmigration is promoted.

amiloride-sensitive event. Here, the ENaC, which is expressed in endothelia (Kusche-Vihrog et al., 2008), is the most promising candidate. Although amiloride potentially inhibits other transporters/channels, such as the Na^+/Ca^{2+} exchanger, the applied concentration of amiloride (1 µM) is known to block specifically ENaC. The IC_{50} of amiloride for ENaC is 0.1 µM (Canessa et al., 1994), while it is 1.76 mM for the Na^+/Ca^{2+} exchanger (Antolini et al., 1993). As amiloride and its analogs are frequently used in treatment of hypertension, the described protective effect of ENaC inhibition on the endothelial pressure response may support the clinical effect of amiloride. Given that ENaC is especially linked to vascular salt sensitivity and hypertension (Lenders et al., 2015; Warnock et al., 2014), a prospective investigation of the detailed mechanism of ENaC-mediated pressure sensing might help to determine the development of hypertension and other cardiovascular diseases. Two possibilities could account for an effect of ENaC on intracellular Ca^{2+}. First, ENaC is involved in plasma membrane potential regulation (Chifflet et al., 2005), which could influence gating of voltage-dependent Ca^{2+} channels, leading to GsMTx4-sensitive Ca^{2+} entry (Spassova et al., 2004). Second, a pressure-induced Na^+ entry via amiloride-sensitive ENaC is likely to counteract the driving force for the Na^+/Ca^{2+} exchanger. By this means, Ca^{2+} export from the cytosol to the extracellular space is reduced and, subsequently, intracellular Ca^{2+} concentration increases. The resulting increase in intracellular Ca^{2+} may further induce storage-operated Ca^{2+} entry via TRP channels (Ichikawa and Inoue, 2014; Nielsen et al., 2014). Nevertheless, the current data do not allow an unequivocal identification of ENaC as the pressure sensing element in endothelia. Still, it might also be possible that ENaC (and other amiloride/benzamil-sensitive targets) represents just another link in the pressure-sensing cascade. A detailed analysis of the signaling pathway, however, is still missing. It is important to note that one still cannot exclude that ENaC is just one step in the signaling cascade downstream of the real pressure sensors. Alternative candidates in the search for pressure sensors, ranging from motor proteins to the tensegrity model of the cytoskeleton, will need to be investigated (Ingber, 2003; Kim et al., 2015; Luo et al., 2012). Integrins, another family of membrane proteins that contribute to endothelial mechanotransduction (Zaragoza et al., 2012), can most likely be excluded from the list of possible pressure sensors. This is because, although it has been shown before that actin polymerization and myosin activation lead to an altered focal adhesion activity and vice versa (Vicente-Manzanares et al., 2009), we did not find any increase in integrin β1 activation in response to pressure. Hence, integrin signaling might therefore be part of stretch-dependent signaling caused by an increase in shear stress or wall tension (Macek et al., 2014), but not a part of the pressure-induced signaling cascade.

This leads to the question of how exactly cells can sense hydrostatic pressure. As aqueous liquids are virtually incompressible, a pressure-sensing mechanism in absence of a gas–liquid interface is still an enigma. Although the presented data clearly indicate that hydrostatic pressure acts as an additional and independent stimulus, this does not explain the molecular mechanism of pressure-dependent signaling. Three mechanisms are likely to facilitate pressure sensation. First, pressure might induce changes in cell shape. This deformation might directly affect the mechanical integrity (tensegrity) of the cell and lead to an alteration of mechanosensitive ion channel activity. This hypothesis is supported by work of Sorce and Charras who have shown that mammalian cells generate intracellular hydrostatic pressure that can be of a spatially heterogeneous nature due to the hydrogel-like character of the viscoelastic cytoplasm (Charras et al., 2005; Sorce et al., 2015). This means that pressure, although it acts isotropically on cells, might have locally distinct effects on membrane/cell shape. Second, pressure has been shown to modify the length of hydrogen bonds and thereby the conformation of biomolecules (Nisius and Grzesiek, 2012; Oger and Jebbar, 2010). However, this effect has so far only been documented for very high hydrostatic pressure levels that far exceed those typically found in human vasculature. The third – and most likely – mechanism of pressure sensing might be a phase shift in the lipid organization of the plasma membrane. It has been shown that under increasing pressure, plasma membrane dynamics shift from a fluid-liquid crystalline state into a gel-like state and that this directly affects transport across the plasma membrane (Nirmalanandhan et al., 2015). This plasma membrane phase shift is likely to affect MSCs and thereby induce the pressure-dependent signaling. Additionally, the MSCs are likely candidates in the search for plasma membrane-anchored pressure

Journal of Cell Science (2018) 131, jcs206920. doi:10.1242/jcs.206920

sensors, as these channels also react to other mechanical stimuli such as shear and tensile stress (Nilius and Droogmans, 2001). Our experiments here verify this hypothesis. Since blocking of MSC activity inhibited the endothelial pressure response completely, it can be concluded that MSCs represent the key player in pressure sensation.

The downstream signaling events induced by an increase in hydrostatic pressure, are much less controversial. Phosphorylation of the regulatory light chain of myosin II plays a critical role in controlling actomyosin contractility in both smooth muscle and non-muscle cells (Kamm and Stull, 1985; Moussavi et al., 1993; Somlyo and Somlyo, 1994). Myosin light chain kinase is regulated via Ca^{2+}/calmodulin and is known to be a major kinase that is involved in myosin activation (Totsukawa et al., 2000, 2004). Hence, the rapid pressure-induced myosin activation is mediated via a Ca^{2+}-dependent phosphorylation of MLC. Consequently, this leads to a reversible increase in line tension within the cortex, characterized by cortical stiffening of the endothelial cell (Fig. 8). Surprisingly, the increase in endothelial stiffness in response to acute pressure application was not associated with a barrier breakdown, which was what has been previously suggested (Huveneers et al., 2015). Apparently the pathologic phenotype of the stiff endothelial cell syndrome (Lang, 2011) might need some time to establish, supporting the hypothesis of non-harmful pressure effects during transient changes in pressure load. Since endothelial nitric oxide synthase (eNOS) is activated via Ca^{2+}/calmodulin (Kuchan and Frangos, 1994), the increased intracellular Ca^{2+} levels during the early response to pressure might activate eNOS and thereby support barrier function. Furthermore, α-filamin contributes to the VE-cadherin-dependent barrier function (Griffiths et al., 2011). Since we found an increased α-filamin expression and concurrent stable VE-cadherin signals, this might explain the intact endothelial barrier function during the acute pressure response.

Prolonged exposure to elevated pressure loads includes a shift from the myosin response to actin polymerization. The increase in cortical actin filament density results in a comparable stiffening of the cell cortex that was, however, not reversible (Fig. 8). There is evidence that myosin II-based contractility is the force that drives the assembly of stress fibers (Burridge and Chrzanowska-Wodnicka, 1996; Chen et al., 2008; Sakurada et al., 1998). Thus, it is tempting to conclude that prolonged activation of MLC (during the initial pressure application) represents the onset of the endothelial response to chronically elevated pressure. The chronic response finally is additionally characterized by an increased endothelial permeability. TEER drops and neutrophil transmigration increases, which is consistent with previously described effects of cell mechanics on barrier function (Fels and Kusche-Vihrog, 2018; Huveneers et al., 2015). Interestingly, chronic pressure application seems to mimic inflammatory conditions, since chronic pressure application increases TEM rates to levels of the TNFα-treated group. Nevertheless, there might even be a positive feature in actin polymerization-driven chronic response to pressure. It has been shown before that increased actin polymerization reduces mechanosensitivity (Glogauer et al., 1997) but simultaneously protects endothelia against mechanical-induced injury (Schnittler et al., 2001). Hence, endothelia might sacrifice mechanosensitivity for a persistent protection of mechanical integrity.

Taken together, we show that hydrostatic pressure acts as a physiological stimulus on endothelial cells. It serves as a stimulus that is independent of shear stress and wall tension. While chronic pressure elevations lead to a global increase in F-actin formation and loss of endothelia barrier function, an acute elevation of hydrostatic pressure induces Ca^{2+} entry via MSCs that activates MLC in the cell cortex but keeps barrier integrity intact. There is strong evidence that the ENaC represents the endothelial pressure sensor.

MATERIALS AND METHODS

Cell culture

Bovine aortic endothelial cells (GM7373, delivered by German Collection of Microorganisms and Cell Cultures; Grinspan et al., 1983), the hybridoma wild-type mock-transfected endothelial cell line EA.hy293 (ATCC CRL-2922) (Edgell et al., 1983), EA.hy 293 ENaC-knockdown cells (Jeggle et al., 2013) and the murine microvascular cell line bEnd5 (96091930, Sigma-Aldrich) were used in this study. Additionally, a GM7373 cell line stably transfected with MLCb–GFP (pEGFP-N1 vector backbone) was generated using FuGene6 transfection reagent (Promega, Madison, NY) as described previously (Kronlage et al., 2015). Cells were cultured in T-25 culture flasks (Becton Dickinson, Heidelberg, Germany), and incubated at 37°C in 5% CO_2 and 100% humidity. Minimal essential medium supplemented with 10% fetal calf serum (PAA Clone, Freiburg, Germany) and 1% non-essential amino acids was used for culture. For experiments, cells from passages 5–18 were seeded either on glass coverslips or on µ-slides I 0.8 Luer (IBIDI, Martinsried, Germany) 24–72 h prior to experiments and used after reaching confluence. All samples for an individual experiment (ambient, 1 h and 24 h) were analyzed on the same day. Hence, confluence was always mature and comparable between samples. In experiments including 24 h pressure incubation, control cells were kept outside the pressure chamber (but within the incubator) at ambient pressure, while the 1 h pressurized samples were only exposed to elevated pressure during the last hour of the respective experiment.

HUVECs were prepared from human umbilical cord veins according to a previously described method (Jaffe et al., 1973) with some minor modifications. Umbilical cords were obtained from full-term, natural delivery cases. (The university ethics review board granted approval for the study, which conforms to the declaration of Helsinki. Informed consent was obtained for the use of the umbilical cords for the isolation of the HUVECs). Cells were grown to confluence on 0.2% gelatin-coated T-25 culture flasks (Becton Dickinson) in a medium composed of Earle's M199 (Gibco, Freiburg, Germany), 10% fetal calf serum (PAA Clone), 1% growth supplement (self-prepared from bovine retina tissue) and 50 U/ml heparin (Biochrom, Berlin, Germany). Cells between passages 1–3 were seeded on fibronectin-coated 24 mm coverslips (Roche, Berlin, Germany) and used for experiments. If not mentioned otherwise, all experiments were performed at 37°C in HEPES buffer (in mM: HEPES 10, glucose 5, $CaCl_2$ 1, $MgCl_2$ 1, KCl 5, NaCl 140; pH 7.4).

A conditionally immortalized Hoxb8 LA-GFP neutrophil precursor cell line, kindly provided by Johannes Roth and Thomas Vogl (Institute of Immunology, University of Münster, Münster, Germany) (Wales et al., 2016), were cultured in RPMI 1640 medium, supplemented with 1% L-glutamine, 10% FCS, 1% SCF-containing CHO-derived supernatant, 30 µM β-mercaptoethanol and 1 µM β-estradiol as described previously (Wales et al., 2016; Wang et al., 2006). To differentiate the precursor cells into neutrophils, medium was replaced with β-estradiol-lacking cell culture medium, and cells were cultured for an additional 4 days until they were fully differentiated. All cell lines were checked for identity by visual inspection of morphologies and tested negative in mycoplasma tests using the following primers: RWS2534, 5′-CGCCTGAGTAGTACGTTCGC-3′; RWS2535, 5′-CGCCTGAGTAGTACGTACGC-3′; RWS2536, 5′-TGCC-TGAGTAGTACATTCGC-3′; RWS2537, 5′-CGCCTGGGTAGTACATT-CGC-3′; RWS2538, 5′-CGCCTGAGTAGTAGTCTCGC-3′; RWS2539, 5′-TGCCTGGGTAGTACATTCGC-3′; RWS2540, 5′-GCGGTGTGTAC-AAGACCCGA-3′; RWS2541, 5′-GCGGTGTGTACAAAACCCGA-3′; RWS2542, 5′-GCGGTGTGTACAAACCCCGA-3′.

Atomic force microscopy

AFM measurements were performed using a Nanowizard III microscope (JPK Instruments, Berlin, Germany). The SmallCell™ closed liquid cell

Journal of Cell Science (2018) 131, jcs206920. doi:10.1242/jcs.206920

(JPK Instruments) was used for all experiments. In acute pressure experiments in living endothelial cells, a targeted field of 100×100 µm was scanned before and after elasticity measurements (256×256 pixels per image) using a gold-coated cantilever with 10 µm polystyrene spherical probes, a nominal spring constant of 0.01 N/m (Novascan Technologies, Ames, USA) and a loading force of 1 nN or less, for the determination of the surface topography of the cell. To compare the acute versus chronic pressure effects, cells were fixed with 3% glutaraldehyde for 15 min to avoid reversal effects and subsequently measured with AFM. It was shown previously that fixed endothelial cells retain cortical actin-based nanomechanics (Grimm et al., 2014; Targosz-Korecka et al., 2015).

The elasticity of the cortical network of actin filaments was measured by nanoindentation spectroscopy (Carl and Schillers, 2008; Kasas and Dietler, 2008). Silicon nitride gold-coated cantilevers (Novascan Technologies) with 10 µm polystyrene spherical probes (nominal spring constant of 0.01 N/m) were used for all elasticity measurements. Force–distance curves were obtained every 5 min with a tip velocity of 1 µm/s and loading forces of 300 pN. Force–distance curves were processed using JRobust software (Hermanowicz et al., 2014).

Using this technique, the cell is indented by a spherical probe, and the penetration depth is measured together with the restoring force acting on the indenter. Sneddon's theory predicts a monomial dependence of the force F on the indentation Δz (Sneddon, 1965) of:

$$F(\Delta z) = \frac{4}{3}\frac{E}{1-\nu^2}\sqrt{R}(\Delta z)^{3/2},$$

where E is the elasticity parameter of the cell cortex (Young's modulus), R is the radius of the spherical probe, and ν is the Poisson ratio of the sample (assumed to be 0.5, meaning perfect incompressibility). Fitting this formula to a force–indentation curve gives the numerical value of the elasticity parameter of the sample. We analyzed the first 100 nm strain of the force–indentation curve, as this part is known to correspond to the cortical actin cytoskeleton (Fels et al., 2012; Kasas et al., 2005; Oberleithner et al., 2009). Additionally, based on the shape of the acquired force–distance curves, we confirmed that the extent of indentation did not exceed 300–500 nm, which is ∼10% of the cell height. We used the term 'Young's modulus' for presenting our absolute data values. Relative changes in Young's modulus are described as 'stiffness'.

Cell volume changes were analyzed as described previously by Korchev et al. (2000). In brief, AFM topography images show the color-coded cell height. Calculating the volume of each pixel in a region of interest (cell) gives the absolute volume of the cell.

Pressure chambers

Two different approaches for acute and chronic hydrostatic pressure incubation were used. Measurements on long-term pressurized cells were performed by using a pressure chamber made in-house. A 7.5 mm thick Plexiglas chamber that fitted into a standard cell culture incubator was used (Fig. 1A). An inlet hose controlled by a stopcock supplied a humidified 5% CO_2/air mixture. Constant pressure ranging from 0 to 160 mmHg (21 kPa) could be achieved by opening the valve and allowing air to fill the chamber to the appropriate level. Chamber pressure was continuously monitored with a digital manometer. Atmospheric pressure (∼760 mmHg, 101 kPa) was used as a reference value (herein referred to as ambient pressure) when no exogenous hydrostatic pressure was applied. For all AFM measurements and confocal imaging of live cells, acute pressurization was performed in a tightly sealed fluid chamber, placed on the base of the dual-probe setup (Fig. 1B). We used a small-volume, closed liquid cell (The SmallCell™, JPK Instruments). A rubber seal was glued to the fluid cell and pressed onto the coverslip, forming a tight fluid chamber. After filling the chamber with buffer via perfusion tubes, one of the tubes was closed, and a reservoir connected to the other tube (variable height reservoir) was raised up to a height of 136 cm, which corresponds to a hydrostatic pressure of 100 mmHg (13 kPa). Pressure levels above 100 mmHg could not be achieved in the live-cell imaging pressure chamber due to leaky sealing at 120 mmHg (or higher). Designed in this way, the pressure chamber allowed us to not induce any shear stress or wall tension. The AFM laser wavelength of 850 nm did not interfere with fluorescence microscopy. Laser ablation experiments and Ca^{2+} measurements were performed in µ-slides with confluent monolayers of endothelial cells. Similar to the design of the AFM pressure chamber, the outflow was closed while the inflow was connected to a hydrostatic reservoir (Fig. 1B).

We also tested the influence of 24 h pressurization on proliferation. For this, we seeded a defined number of cells (5000/cm^2) on 35 mm dishes and placed them either in the standard incubator or in the cell culture pressure chamber, respectively. Cells were trypsinized and counted after 24 and 48 h. We were not able to detect any significant effect on cell proliferation within the first 24 h of pressure incubation, while the cells appeared to proliferate more after 48 h of pressure application (Fig. S1A). The stimulating effect of pressure on proliferation reported by others (see above) may be explained by the duration of pressure application. In most of the mentioned studies, cells were kept at pressurized conditions for more than 72 h. To exclude any effects due to possible hypoxia, experimental control series were performed for the acute as well as the chronic pressure chamber. Samples of the culture medium were obtained from experimental dishes and immediately analyzed for pH, pCO_2 and pO_2. Media taken from both chambers showed no significant variations in these parameters compared to those taken from non-pressurized control experiments (Table S1). Furthermore, we tested for any changes in cortical stiffness when there were no alterations in pressure. As shown in the tracings in Fig. S1B, the cortical stiffness of GM7373 cells and HUVECs does not change over a timecourse of 150 min, which corresponds to the average duration of experiments. Hence, we conclude that our experimental approach is not influenced by hypoxia or proliferation-dependent artifacts.

Immunofluorescence microscopy

Confocal fluorescence microscopy was used for the visualization of pressure-dependent effects on the cytoskeletal structures in the cortex of endothelial cells. For visualization of cytoskeletal actin-derived rearrangements induced by long-term pressure application, cells were fixed with 3% paraformaldehyde in PBS for 15 min immediately after chronic pressure exposure, and permeabilized at room temperature with 0.1% Triton X-100 (Sigma-Aldrich, Berlin, Germany). To prevent nonspecific antibody binding, endothelial cells were pretreated with 10% goat normal serum (ThermoFisher, Darmstadt, Germany) at room temperature for 30 min and then incubated for 60 min with phalloidin tetramethylrhodamine B isothiocyanate (TRITC–phalloidin; Sigma-Aldrich), or antibodies against myosin light chain 2 (1:100, ab48003, Abcam, Cambridge, UK) phospho-myosin light chain 2 (1:100, PA5-17727, ThermoFisher), non-muscle myosin heavy chain IIa (1:100, ab55456, Abcam), α-actinin-1 (1:100, A5044, Sigma-Aldrich), α-filamin (MAB1680, Merck, Darmstadt, Germany), cofilin (1:100, sc33779, SCBT, Heidelberg, Germany), phospho-cofilin (1:100, sc271921, SCBT), active integrin β1 (1:50, ab202641, Abcam) or anti-VE-cadherin antibody (1:100, 2158S, Cell Signaling, Danvers, USA). A secondary goat anti-rabbit-IgG conjugated to Alexa Fluor 568, goat anti-rabbit-IgG conjugated to Alexa Fluor 647 or goat anti-mouse-IgG conjugated to Alexa Fluor 488 was then added for 60 min. All secondary antibodies were diluted 1:400. Furthermore, all samples were stained with DAPI to facilitate the identification of the correct focal plane. Finally, coverslips were mounted in mounting medium (DAKO, Hamburg, Germany).

Fluorescence images were acquired using a fully automated iMIC2 microscope from FEI/Till Photonics, equipped with a spinning disk unit (Andromeda) using an Olympus 60× NA 1.49 objective and an Andor iXon Ultra 987 EMCCD camera. The fluorophores were excited at 488 nm, 561 nm or 405 nm, respectively. Sequential scanning was applied to avoid acquiring concurrent fluorescence signals from two fluorophores.

Cortical fluorescence intensity was measured by quantification of fluorescence intensity in the topmost focal plane above the nucleus. Although the z-resolution (step size 300 nm) of confocal microscopy is limited, this method allows an almost exclusive detection of apical cortical fluorophores. Peripheral actin or myosin at the borders of the cells, cannot be used to quantify cortical intensity because artifacts caused by the junctional actin ring cannot be excluded. To estimate basal

expression levels, basal fluorescence intensity (i.e. below the nuclear focal plane) was quantified. For analysis of fluorescence intensities, all images had the background subtracted. The mean fluorescence intensity of pressurized samples was normalized to values measured at ambient pressure.

F-actin:G-actin ratio and western blotting

The ratio of G-actin to F-actin was determined with the G-actin/F-actin *In Vivo* Assay Kit (Cytoskeleton, Denver, USA) based on the manufacturer's protocol. Briefly, cells were lysed in F-actin stabilization buffer and cell lysates centrifuged at 100,000 ***g*** to separate the F-actin from the G-actin pool. The G-actin fraction was diluted 10-fold and re-quantified during analysis. Equal amounts of samples were loaded into lanes of polyacrylamide gels and analyzed by western blotting using a pan-actin antibody. For the control of proper F- and G-actin separation, the nuclear pore complex protein NUP62 (62 kDa) was used as a reference protein (Mab414 antibody, Abcam, Cambridge, UK). Owing to the centrifugation step, this protein normally mostly appears in the F-actin fraction.

Whole-cell extracts (for myosin detection), or F- and G-actin-containing cell fractions were separated by SDS-PAGE and transferred to a polyvinylidene-difluoride membrane using a wet-transfer apparatus according to the manufacturer's protocol (Bio-Rad, Munich, Germany). After incubation with 5% non-fat milk in TBST (10 mM Tris-HCl, 150 mM NaCl, 0.5% Tween 20, pH 8.0) for 60 min, the membrane was incubated with antibodies against myosin light chain (1:100, ab48003, Abcam), phospho-myosin light chain (1:50, PA5-17727, ThermoFisher), NUP62 (1:100, WH0023636M2, Sigma-Aldrich), tubulin (1:200, 14-4502-82, ThermoFisher), acetylated tubulin (1:100, T7451, Sigma-Aldrich), vimentin (1:100, ab8978, Abcam), VE-cadherin (1:100, 2158S, Cell Signaling), GAPDH (1:200, ab125247, Abcam) or β-actin (1:100, ab125248, Abcam) at room temperature for 1 h. Membranes were washed four times for 7 min and incubated with anti-rabbit-IgG or anti-mouse-IgG secondary antibodies conjugated to horseradish peroxidase for 1 h. Blots were washed five times with TBST, and images were recorded on a chemiluminescent immunodetection system (Bio-Rad) according to the manufacturer's protocol. The authors are aware of a general uncertainty with GAPDH as a loading control (Eisenberg and Levanin, 2013), but we found GAPDH was stably expressed in our samples. As tubulin was a gene of interest in this particular assay, it was more appropriate to normalize intensities of respective bands to GAPDH signal during western blot quantification.

Laser ablation

Ablation experiments were performed on an automated iMIC-based microscope (FEI/Till Photonics) equipped with a 100×, 1.4 NA objective (Olympus), a diode-pumped solid state laser at 491 nm (75 mV; Calypso; Cobolt) and a pulsed 355 nm UV laser (DPSL-355/14, Rapp OptoElectronic). GM7373 MLC–GFP cells cultured on μ-slides, were mounted on the iMIC stage. The first port of the μ-slides was connected to a hydrostatic reservoir (similar to the AFM SmallCell), while the second port was closed to prevent shear flow during pressure elevation (Fig. 1B). Ablation of myosin filaments, labeled by MLCb–GFP, was performed as described previously (Klingner et al., 2014). In brief, apical acto-myosin filaments were severed by using the pulsed UV laser. Retraction of single filaments was recorded at a rate of one frame every 100–200 ms. To quantify the retraction velocity, kymographs were generated perpendicular to the performed cut (i.e. in the direction of the retraction). The linear slope within the first second of the retraction kymographs was measured with FIJI software (National Institutes of Health). Prior to pressure application, retraction velocities of acto-myosin filaments of 5–10 cells were recorded at ambient pressure. Subsequently, the hydrostatic reservoir was raised to generate a pressure of 100 mmHg in addition to ambient pressure. After 60 min of pressure application, retraction velocities of another 5–10 cells (different cells than cells measured at ambient pressure) were quantified. All ablation experiments were performed at room temperature (RT) in HEPES-buffered solution (pH 7.4).

Intracellular Ca^{2+} measurements

Confluent cells, grown on μ-slides, were loaded with 5 μg/ml FLUOFORTE® (Enzo) in HEPES buffer supplemented with 0.2% Pluronic F-127 (final) for 30 min at RT. Excess dye was subsequently washed off. Cell culture vessels were transferred to the iMIC setup (see above) and connected to the hydrostatic head. To assess changes in baseline $[Ca^{2+}]_i$ levels, cell images were acquired every 2 min for 10 min at ambient pressure and subsequently exposed to an additional 100 mmHg for up to 90 min. For quantification of Ca^{2+} oscillations, images were acquired every 4 s for 10 min at ambient pressure (control) followed by the first 10 min directly after the increase in pressure. Subsequent to acquisition, we analyzed all images with FIJI software. To exclude false-positive peak detection, Ca^{2+} sparks were considered as relevant if peak intensity was ≥1.15 fold of pre-peak baseline. Prior to peak intensity analysis, images were corrected by background subtraction. As for the ablation experiments, all Ca^{2+} measurements were conducted at RT in HEPES-buffered solution (pH 7.4).

Transendothelial electrical resistance

TEER was measured using an electrical volt/ohm-meter equipped with a chopstick electrode (WPI, Sarasota, FL, USA). Cells were seeded on transwell inserts (Corning Costar, Sigma-Aldrich) and grown until they reached confluence. TEER was measured before and after pressure application.

Quantification of VE-cadherin

To quantify changes in VE-cadherin organization, we calculated the area:contour length ratio as a measure of distribution of VE-cadherin at cell–cell junctions. *Z*-stacks of VE-cadherin stained endothelial cells were converted into binary images (0, no signal; 1, VE-cadherin present). Subsequently, the length of cell contacts were determined, as well as the area occupied by the VE-cadherin signal. Afterwards, the total VE-cadherin area (pixels) was divided by total length of cell–cell contacts to measure the area:contour length ratio. Data were normalized to that in the ambient control.

Transmigration assay

bEnd5 endothelial cells were seeded onto polycarbonate membrane transwell inserts (Corning Costar) with pore sizes of 3 μm. Cells were grown until they reached confluence, as validated by TEER measurements (Fig. S1C). On the day of experiments, the medium was supplemented with 50 ng/ml C5a (R&D Systems, Wiesbaden, Germany) and 10^6 differentiated Hoxb8 neutrophils/cm^2 were added to the upper compartment. Neutrophils were allowed to transmigrate through the endothelial monolayer for 1 h. Subsequently, the number of neutrophils in the lower compartment was counted using a Neubauer chamber (Celeromics, Cambridge, UK). Nine different conditions were tested: (1) ambient pressure, (2) 1 h at 100 mmHg (i.e. 1 h pressure incubation with concurrently added neutrophils), (3) 24 h at 100 mmHg (i.e. 23 h pressure incubation+1 h pressure incubation with added neutrophils), (4) ambient pressure+1 μM amiloride, (5) 1 h at 100 mmHg+1 μM amiloride, (6) 24 h at 100 mmHg+1 μM amiloride, (7) ambient pressure+10 ng/ml TNFα, (8) 1 h at 100 mmHg+10 ng/ml TNFα, and (9) 24 h at 100 mmHg+10 ng/ml TNFα.

Statistical analysis

Values were pooled from at least four independent experiments. All replicates are biological replicates. Bar diagrams, showing mean values with the s.e.m., are used for parametric data sets. Figures with non-parametric data are shown as box blots, presenting 25 and 75 percentiles, mean values (square symbol), median (horizontal line) and 1.5× the interquartile range (whiskers). Statistical comparison between two groups was performed by using *t*-test or a Mann–Whitney test in case of parametric or nonparametric distribution, respectively. If more than two conditions were compared, either ANOVA with a Bonferoni post-test (parametric), or a Kruskal–Wallis test with subsequent Mann–Whitney test (non-parametric) was applied. As soon as one group within a specific data set showed non-parametric distribution, the whole data set was considered as non-parametric. Compared data sets were considered as significantly different at $P<0.05$. OriginPro 2015G (OriginLab Corporation) was used to calculate all statistics. A complete list of statistical tests, including the exact *P*-value, the number of analyzed cells (*n*) as well as the applied test is given in Table S2.

Acknowledgements

We gratefully acknowledge the networking activities of the COST action TD 1002. The authors appreciate the technical support from Jacek Szczerbinski (ETH, Zürich,

Switzerland), Marianne Wilhelmi (Institute of Physiology II, University of Münster, Germany), Annette Janning and Ingrid Otto-Valk (Intitute of Cell Dynamics and Imaging, University of Münster, Germany), as well as Thomas Westhoff, Ludger Sasse and Andreas Kolkmann (research workshops, University Hospital Münster, Germany).

Competing interests
The authors declare no competing or financial interests.

Author contributions
Conceptualization: V.P., R.W.-S., H.O., J.F.; Methodology: J.F.; Validation: V.P., B.F., C.S.S., I.L., D.P., C.K., J.F.; Formal analysis: V.P., B.F., C.S.S., J.F.; Investigation: V.P., B.F., C.S.S., I.L., D.P., C.K., J.F.; Resources: R.W.-S., H.O.; Data curation: R.W.-S., H.O.; Writing - original draft: V.P., R.W.-S., H.O., J.F.; Writing - review & editing: V.P., B.F., C.S.S., I.L., C.K., R.W.-S., H.O., J.F.; Visualization: V.P., B.F., C.S.S., J.F.; Supervision: J.F.; Project administration: R.W.-S., H.O., J.F.; Funding acquisition: R.W.-S., H.O., J.F.

Funding
Work was supported by the Cells-in-Motion Cluster of Excellence, the Program für innovative medizinische Forschung (I-FE 220904 to J.F.) and by the Deutsche Forschungsgemeinschaft (SFB 1009 to R.W.-S., Koselleck-grant OB 63/18 to H.O.).

Supplementary information
Supplementary information available online at
http://jcs.biologists.org/lookup/doi/10.1242/jcs.206920.supplemental

References
Acevedo, A. D., Bowser, S. S., Gerritsen, M. E. and Bizios, R. (1993). Morphological and proliferative responses of endothelial cells to hydrostatic pressure: role of fibroblast growth factor. *J. Cell Physiol.* **157**, 603-614.

Antolini, M., Trevisi, L., Debetto, P. and Luciani, S. (1993). Effect of amiloride on sodium-calcium exchange activity in rat cardiac myocytes. *Pharmacol. Res.* **27**, 227-232.

Bowman, C. L., Gottlieb, P. A., Suchyna, T. M., Murphy, Y. K. and Sachs, F. (2007). Mechanosensitive ion channels and the peptide inhibitor GsMTx-4: history, properties, mechanisms and pharmacology. *Toxicon* **49**, 249-270.

Burridge, K. and Chrzanowska-Wodnicka, M. (1996). Focal adhesions, contractility, and signaling. *Annu. Rev. Cell Dev. Biol.* **12**, 463-518.

Canessa, C. M., Schild, L., Buell, G., Thorens, B., Gautschi, I., Horisberger, J.-D. and Rossier, B. C. (1994). Amiloride-sensitive epithelial Na^+ channel is made of three homologous subunits. *Nature* **367**, 463-467.

Carl, P. and Schillers, H. (2008). Elasticity measurement of living cells with an atomic force microscope: data acquisition and processing. *Pflugers Arch.* **457**, 551-559.

Charras, G. T., Yarrow, J. C., Horton, M. A., Mahadevan, L. and Mitchison, T. J. (2005). Non-equilibration of hydrostatic pressure in blebbing cells. *Nature* **435**, 365-369.

Chen, X., Pavlish, K. and Benoit, J. N. (2008). Myosin phosphorylation triggers actin polymerization in vascular smooth muscle. *Am. J. Physiol Heart Circ. Physiol.* **295**, H2172-H2177.

Chifflet, S., Hernández, J. A. and Grasso, S. (2005). A possible role for membrane depolarization in epithelial wound healing. *Am. J. Physiol. Cell Physiol.* **288**, C1420-C1430.

Codan, B., Martinelli, V., Mestroni, L. and Sbaizero, O. (2013). Atomic force microscopy of 3T3 and SW-13 cell lines: an investigation of cell elasticity changes due to fixation. *Mater. Sci. Eng C. Mater. Biol. Appl.* **33**, 3303-3308.

Davies, P. F. (2009). Hemodynamic shear stress and the endothelium in cardiovascular pathophysiology. *Nat. Clin. Pract. Cardiovasc. Med.* **6**, 16-26.

Edgell, C. J., McDonald, C. C. and Graham, J. B. (1983). Permanent cell line expressing human factor VIII-related antigen established by hybridization. *Proc. Natl. Acad. Sci. USA* **80**, 3734-3737.

Eisenberg, E. and Levanon, EY. (2013). Human housekeeping genes, revisited. *Trends Genet.* **29**, 569-574.

Elder, B. D. and Athanasiou, K. A. (2009). Hydrostatic pressure in articular cartilage tissue engineering: from chondrocytes to tissue regeneration. *Tissue Eng Part B Rev.* **15**, 43-53.

Ezzati, M., Lopez, A. D., Rodgers, A., Vander, H. S. and Murray, C. J. L. (2002). Selected major risk factors and global and regional burden of disease. *Lancet* **360**, 1347-1360.

Fels, J. and Kusche-Vihrog, K. (2018). Endothelial nanomechanics in the context of endothelial (Dys)function and inflammation. *Antioxid. Redox. Signal*. [In Press].

Fels, J., Jeggle, P., Kusche-Vihrog, K. and Oberleithner, H. (2012). Cortical actin nanodynamics determines nitric oxide release in vascular endothelium. *PLoS. ONE* **7**, e41520.

Fels, J., Jeggle, P., Liashkovich, I., Peters, W. and Oberleithner, H. (2014). Nanomechanics of vascular endothelium. *Cell Tissue Res.* **355**, 727-737.

Fels, B., Nielsen, N. and Schwab, A. (2016). Role of TRPC1 channels in pressure-mediated activation of murine pancreatic stellate cells. *Eur. Biophys. J.* **45**, 657-670.

Gardinier, J. D., Gangadharan, V., Wang, L. and Duncan, R. L. (2014). Hydraulic pressure during fluid flow regulates purinergic signaling and cytoskeleton organization of osteoblasts. *Cell Mol. Bioeng.* **7**, 266-277.

Glogauer, M., Arora, P., Yao, G., Sokholov, I., Ferrier, J. and McCulloch, C. A. (1997). Calcium ions and tyrosine phosphorylation interact coordinately with actin to regulate cytoprotective responses to stretching. *J. Cell Sci.* **110**, 11-21.

Griffiths, G. S., Grundl, M., Allen, J. S., III and Matter, M. L. (2011). R-Ras interacts with filamin a to maintain endothelial barrier function. *J. Cell Physiol.* **226**, 2287-2296.

Grimm, K. B., Oberleithner, H. and Fels, J. (2014). Fixed endothelial cells exhibit physiologically relevant nanomechanics of the cortical actin web. *Nanotechnology* **25**, 215101.

Grinspan, J. B., Mueller, S. N. and Levine, E. M. (1983). Bovine endothelial cells transformed in vitro by benzo(a)pyrene. *J. Cell Physiol.* **114**, 328-338.

Guo, D., Liang, S., Wang, S., Tang, C., Yao, B., Wan, W., Zhang, H., Jiang, H., Ahmed, A., Zhang, Z. et al. (2016). Role of epithelial Na+ channels in endothelial function. *J. Cell Sci.* **129**, 290-297.

Hahn, C. and Schwartz, M. A. (2009). Mechanotransduction in vascular physiology and atherogenesis. *Nat. Rev. Mol. Cell Biol.* **10**, 53-62.

Hermanowicz, P., Sarna, M., Burda, K. and Gabryś, H. (2014). AtomicJ: an open source software for analysis of force curves. *Rev. Sci. Instrum.* **85**, 063703.

Huveneers, S., Daemen, M. J. A. P. and Hordijk, P. L. (2015). Between Rho(k) and a hard place: the relation between vessel wall stiffness, endothelial contractility, and cardiovascular disease. *Circ. Res.* **116**, 895-908.

Ichikawa, J. and Inoue, R. (2014). TRPC6 regulates cell cycle progression by modulating membrane potential in bone marrow stromal cells. *Br. J. Pharmacol.* **171**, 5280-5294.

Ingber, D. E. (2003). Tensegrity II. How structural networks influence cellular information processing networks. *J. Cell Sci.* **116**, 1397-1408.

Jaasma, M. J., Jackson, W. M., Tang, R. Y. and Keaveny, T. M. (2007). Adaptation of cellular mechanical behavior to mechanical loading for osteoblastic cells. *J. Biomech.* **40**, 1938-1945.

Jaffe, E. A., Nachman, R. L., Becker, C. G. and Minick, C. R. (1973). Culture of human endothelial cells derived from umbilical veins. Identification by morphologic and immunologic criteria. *J. Clin. Invest* **52**, 2745-2756.

Jeggle, P., Callies, C., Tarjus, A., Fassot, C., Fels, J., Oberleithner, H., Jaisser, F. and Kusche-Vihrog, K. (2013). Epithelial sodium channel stiffens the vascular endothelium in vitro and in liddle mice. *Hypertension* **61**, 1053-1059.

Kamm, K. E. and Stull, J. T. (1985). The function of myosin and myosin light chain kinase phosphorylation in smooth muscle. *Annu. Rev. Pharmacol. Toxicol.* **25**, 593-620.

Kasas, S. and Dietler, G. (2008). Probing nanomechanical properties from biomolecules to living cells. *Pflugers Arch.* **456**, 13-27.

Kasas, S., Wang, X., Hirling, H., Marsault, R., Huni, B., Yersin, A., Regazzi, R., Grenningloh, G., Riederer, B., Forro, L. et al. (2005). Superficial and deep changes of cellular mechanical properties following cytoskeleton disassembly. *Cell Motil. Cytoskeleton* **62**, 124-132.

Kim, J. H., Ren, Y., Ng, W. P., Li, S., Son, S., Kee, Y.-S., Zhang, S., Zhang, G., Fletcher, D. A., Robinson, D. N. et al. (2015). Mechanical tension drives cell membrane fusion. *Dev. Cell* **32**, 561-573.

Klingner, C., Cherian, A. V., Fels, J., Diesinger, P. M., Aufschnaiter, R., Maghelli, N., Keil, T., Beck, G., Tolić-Nørrelykke, I. M., Bathe, M. et al. (2014). Isotropic actomyosin dynamics promote organization of the apical cell cortex in epithelial cells. *J. Cell Biol.* **207**, 107-121.

Korchev, Y. E., Gorelik, J., Lab, M. J., Sviderskaya, E. V., Johnston, C. L., Coombes, C. R., Vodyanoy, I. and Edwards, C. R. W. (2000). Cell volume measurement using scanning ion conductance microscopy. *Biophys. J.* **78**, 451-457.

Kronlage, C., Schäfer-Herte, M., Böning, D., Oberleithner, H. and Fels, J. (2015). Feeling for filaments: quantification of the cortical actin web in live vascular endothelium. *Biophys. J.* **109**, 687-698.

Kuchan, M. J. and Frangos, J. A. (1994). Role of calcium and calmodulin in flow-induced nitric oxide production in endothelial cells. *Am. J. Physiol.* **266**, C628-C636.

Kusche-Vihrog, K., Sobczak, K., Bangel, N., Wilhelmi, M., Nechyporuk-Zloy, V., Schwab, A., Schillers, H. and Oberleithner, H. (2008). Aldosterone and amiloride alter ENaC abundance in vascular endothelium. *Pflugers Arch.* **455**, 849-857.

Lang, F. (2011). Stiff endothelial cell syndrome in vascular inflammation and mineralocorticoid excess. *Hypertension* **57**, 146-147.

Laudadio, R. E., Millet, E. J., Fabry, B., An, S. S., Butler, J. P. and Fredberg, J. J. (2005). Rat airway smooth muscle cell during actin modulation: rheology and glassy dynamics. *Am. J. Physiol. Cell Physiol.* **289**, C1388-C1395.

Lee, S. Y., Zaske, A. M., Novellino, T., Danila, D., Ferrari, M., Conyers, J. and Decuzzi, P. (2011). Probing the mechanical properties of TNF-alpha stimulated endothelial cell with atomic force microscopy. *Int. J. Nanomedicine.* **6**, 179-195.

Lehoux, S., Castier, Y. and Tedgui, A. (2006). Molecular mechanisms of the vascular responses to haemodynamic forces. *J. Intern. Med.* **259**, 381-392.
Lenders, M., Hofschroer, V., Schmitz, B., Kasprzak, B., Rohlmann, A., Missler, M., Pavenstädt, H., Oberleithner, H., Brand, S.-M., Kusche-Vihrog, K. et al. (2015). Differential response to endothelial epithelial sodium channel inhibition ex vivo correlates with arterial stiffness in humans. *J. Hypertens.* **33**, 2455-2462.
Liu, C. and Montell, C. (2015). Forcing open TRP channels: mechanical gating as a unifying activation mechanism. *Biochem. Biophys. Res. Commun.* **460**, 22-25.
Luo, T., Mohan, K., Srivastava, V., Ren, Y., Iglesias, P. A. and Robinson, D. N. (2012). Understanding the cooperative interaction between myosin II and actin cross-linkers mediated by actin filaments during mechanosensation. *Biophys. J.* **102**, 238-247.
Macek, J. Z., Lisowska, J., Manet, S., Verdier, C., Deplano, V., Geindreau, C., Faurobert, E., Albiges-Rizo, C. and Duperray, A. (2014). CCM proteins control endothelial beta1 integrin dependent response to shear stress. *Biol. Open.* **3**, 1228-1235.
Mandal, A., Shahidullah, M. and Delamere, N. A. (2010). Hydrostatic pressure-induced release of stored calcium in cultured rat optic nerve head astrocytes. *Invest Ophthalmol. Vis. Sci.* **51**, 3129-3138.
Martens, J. C. and Radmacher, M. (2008). Softening of the actin cytoskeleton by inhibition of myosin II. *Pflugers Arch.* **456**, 95-100.
Martin, J. S., Brown, L. S. and Haberstroh, K. M. (2005). Microfilaments are involved in renal cell responses to sustained hydrostatic pressure. *J. Urol.* **173**, 1410-1417.
Martinelli, R., Zeiger, A. S., Whitfield, M., Sciuto, T. E., Dvorak, A., Van Vliet, K. J., Greenwood, J. and Carman, C. V. (2014). Probing the biomechanical contribution of the endothelium to lymphocyte migration: diapedesis by the path of least resistance. *J. Cell Sci.* **127**, 3720-3734.
Matthews, B. D., Overby, D. R., Mannix, R. and Ingber, D. E. (2006). Cellular adaptation to mechanical stress: role of integrins, Rho, cytoskeletal tension and mechanosensitive ion channels. *J. Cell Sci.* **119**, 508-518.
Moussavi, R. S., Kelley, C. A. and Adelstein, R. S. (1993). Phosphorylation of vertebrate nonmuscle and smooth muscle myosin heavy chains and light chains. *Mol. Cell Biochem.* **127-128**, 219-227.
Müller-Marschhausen, K., Waschke, J. and Drenckhahn, D. (2008). Physiological hydrostatic pressure protects endothelial monolayer integrity. *Am. J. Physiol. Cell Physiol.* **294**, C324-C332.
Nielsen, N., Lindemann, O. and Schwab, A. (2014). TRP channels and STIM/ORAI proteins: sensors and effectors of cancer and stroma cell migration. *Br. J. Pharmacol.* **171**, 5524-5540.
Nilius, B. and Droogmans, G. (2001). Ion channels and their functional role in vascular endothelium. *Physiol. Rev.* **81**, 1415-1459.
Nirmalanandhan, V. S., Hurren, R., Cameron, W. D., Gronda, M., Shamas-Din, A., You, L., Minden, M. D., Rocheleau, J. V. and Schimmer, A. D. (2015). Increased pressure alters plasma membrane dynamics and renders acute myeloid leukemia cells resistant to daunorubicin. *Haematologica* **100**, e406-e408.
Nisius, L. and Grzesiek, S. (2012). Key stabilizing elements of protein structure identified through pressure and temperature perturbation of its hydrogen bond network. *Nat. Chem.* **4**, 711-717.
Oberleithner, H., Callies, C., Kusche-Vihrog, K., Schillers, H., Shahin, V., Riethmüller, C., MacGregor, G. A. and de Wardener, H. E. (2009). Potassium softens vascular endothelium and increases nitric oxide release. *Proc. Natl. Acad. Sci USA* **106**, 2829-2834.
Oger, P. M. and Jebbar, M. (2010). The many ways of coping with pressure. *Res. Microbiol.* **161**, 799-809.
O'Hagan, R., Chalfie, M. and Goodman, M. B. (2005). The MEC-4 DEG/ENaC channel of Caenorhabditis elegans touch receptor neurons transduces mechanical signals. *Nat. Neurosci.* **8**, 43-50.
Ohashi, T., Sugaya, Y., Sakamoto, N. and Sato, M. (2007). Hydrostatic pressure influences morphology and expression of VE-cadherin of vascular endothelial cells. *J. Biomech.* **40**, 2399-2405.
Portran, D., Schaedel, L., Xu, Z., Théry, M. and Nachury, M. V. (2017). Tubulin acetylation protects long-lived microtubules against mechanical ageing. *Nat. Cell Biol.* **19**, 391-398.
Sakurada, K., Seto, M. and Sasaki, Y. (1998). Dynamics of myosin light chain phosphorylation at Ser19 and Thr18/Ser19 in smooth muscle cells in culture. *Am. J. Physiol.* **274**, C1563-C1572.
Salwen, S. A., Szarowski, D. H., Turner, J. N. and Bizios, R. (1998). Three-dimensional changes of the cytoskeleton of vascular endothelial cells exposed to sustained hydrostatic pressure. *Med. Biol. Eng Comput.* **36**, 520-527.
Sappington, R. M., Sidorova, T., Long, D. J. and Calkins, D. J. (2009). TRPV1: contribution to retinal ganglion cell apoptosis and increased intracellular Ca2+ with exposure to hydrostatic pressure. *Invest Ophthalmol. Vis. Sci.* **50**, 717-728.
Schillers, H., Wälte, M., Urbanova, K. and Oberleithner, H. (2010). Real-time monitoring of cell elasticity reveals oscillating myosin activity. *Biophys. J.* **99**, 3639-3646.
Schnittler, H.-J., Schneider, S. W., Raifer, H., Luo, F., Dieterich, P., Just, I. and Aktories, K. (2001). Role of actin filaments in endothelial cell-cell adhesion and membrane stability under fluid shear stress. *Pflugers Arch.* **442**, 675-687.
Schnittler, H., Taha, M., Schnittler, M. O., Taha, A. A., Lindemann, N. and Seebach, J. (2014). Actin filament dynamics and endothelial cell junctions: the Ying and Yang between stabilization and motion. *Cell Tissue Res.* **355**, 529-543.
Schwartz, E. A., Bizios, R., Medow, M. S. and Gerritsen, M. E. (1999). Exposure of human vascular endothelial cells to sustained hydrostatic pressure stimulates proliferation. Involvement of the alphaV integrins. *Circ. Res.* **84**, 315-322.
Shimamura, K., Sekiguchi, F. and Sunano, S. (1999). Tension oscillation in arteries and its abnormality in hypertensive animals. *Clin. Exp. Pharmacol. Physiol.* **26**, 275-284.
Smith, R. L., Carter, D. R. and Schurman, D. J. (2004). Pressure and shear differentially alter human articular chondrocyte metabolism: a review. *Clin. Orthop. Relat Res.* **427**, S89-S95.
Sneddon, I. N. (1965). The relation betwee load and penetration in the axisymmetric boussinesq problem for a punch of arbitrary profile. *Int. J. Engng Sci.* **3**, 47-57.
Somlyo, A. P. and Somlyo, A. V. (1994). Signal transduction and regulation in smooth muscle. *Nature* **372**, 231-236.
Sorce, B., Escobedo, C., Toyoda, Y., Stewart, M. P., Cattin, C. J., Newton, R., Banerjee, I., Stettler, A., Roska, B., Eaton, S. et al. (2015). Mitotic cells contract actomyosin cortex and generate pressure to round against or escape epithelial confinement. *Nat. Commun.* **6**, 8872.
Spassova, M. A., Soboloff, J., He, L.-P., Hewavitharana, T., Xu, W., Venkatachalam, K., van Rossum, D. B., Patterson, R. L. and Gill, D. L. (2004). Calcium entry mediated by SOCs and TRP channels: variations and enigma. *Biochim. Biophys. Acta* **1742**, 9-20.
Sumpio, B. E., Widmann, M. D., Ricotta, J., Awolesi, M. A. and Watase, M. (1994). Increased ambient pressure stimulates proliferation and morphologic changes in cultured endothelial cells. *J. Cell. Physiol.* **158**, 133-139.
Szczygiel, A. M., Brzezinka, G., Targosz-Korecka, M., Chlopicki, S. and Szymonski, M. (2011). Elasticity changes anti-correlate with NO production for human endothelial cells stimulated with TNF-alpha. *Pflugers Arch.* **463**, 487-496.
Targosz-Korecka, M., Brzezinka, G. D., Danilkiewicz, J., Rajfur, Z. and Szymonski, M. (2015). Glutaraldehyde fixation preserves the trend of elasticity alterations for endothelial cells exposed to TNF-alpha. *Cytoskeleton* **72**, 124-130.
Tavernarakis, N. and Driscoll, M. (2001). Mechanotransduction in Caenorhabditis elegans: the role of DEG/ENaC ion channels. *Cell Biochem. Biophys.* **35**, 1-18.
Thoumine, O., Nerem, R. M. and Girard, P. R. (1995). Oscillatory shear stress and hydrostatic pressure modulate cell-matrix attachment proteins in cultured endothelial cells. *In Vitro Cell Dev. Biol. Anim.* **31**, 45-54.
Totsukawa, G., Yamakita, Y., Yamashiro, S., Hartshorne, D. J., Sasaki, Y. and Matsumura, F. (2000). Distinct roles of ROCK (Rho-kinase) and MLCK in spatial regulation of MLC phosphorylation for assembly of stress fibers and focal adhesions in 3T3 fibroblasts. *J. Cell Biol.* **150**, 797-806.
Totsukawa, G., Wu, Y., Sasaki, Y., Hartshorne, D. J., Yamakita, Y., Yamashiro, S. and Matsumura, F. (2004). Distinct roles of MLCK and ROCK in the regulation of membrane protrusions and focal adhesion dynamics during cell migration of fibroblasts. *J. Cell Biol.* **164**, 427-439.
Vicente-Manzanares, M., Choi, C. K. and Horwitz, A. R. (2009). Integrins in cell migration–the actin connection. *J. Cell Sci.* **122**, 199-206.
Wales, P., Schuberth, C. E., Aufschnaiter, R., Fels, J., Garcia-Aguilar, I., Janning, A., Dlugos, C. P., Schafer-Herte, M., Klingner, C., Walte, M. et al. (2016). Calcium-mediated actin reset (CaAR) mediates acute cell adaptations. *Elife* **5**, e19850.
Wang, G. G., Calvo, K. R., Pasillas, M. P., Sykes, D. B., Häcker, H. and Kamps, M. P. (2006). Quantitative production of macrophages or neutrophils ex vivo using conditional Hoxb8. *Nat. Methods* **3**, 287-293.
Warnock, D. G., Kusche-Vihrog, K., Tarjus, A., Sheng, S., Oberleithner, H., Kleyman, T. R. and Jaisser, F. (2014). Blood pressure and amiloride-sensitive sodium channels in vascular and renal cells. *Nat. Rev. Nephrol.* **10**, 146-157.
Zaragoza, C., Marquez, S. and Saura, M. (2012). Endothelial mechanosensors of shear stress as regulators of atherogenesis. *Curr. Opin. Lipidol.* **23**, 446-452.
Zhao, Y.-H., Lv, X., Liu, Y.-L., Zhao, Y., Li, Q., Chen, Y.-J. and Zhang, M. (2015). Hydrostatic pressure promotes the proliferation and osteogenic/chondrogenic differentiation of mesenchymal stem cells: the roles of RhoA and Rac1. *Stem Cell Res.* **14**, 283-296.

Supplementary figures

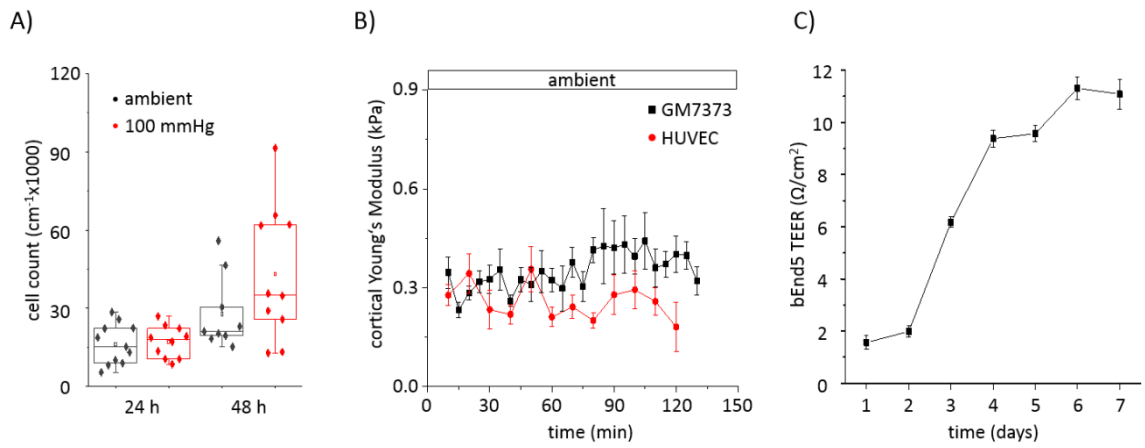

Supplementary figure 1: (A) 5000 cell/cm^2 were seeded on 35 mm dishes and incubated at ambient pressure or 100 mmHg for 24 or 48 h, respectively. Cell counting indicates no effect of pressure on proliferation within the first 24 h. * = significant difference to ambient control. **(B)** Cortical elasticity of living GM7373 (black) or HUVEC cells (red) was quantified at ambient pressure to verify the pressure chamber. **(C)** TEER of bEnd5 seeded on 3 µm pore size polycarbonate transwell inserts. Cells reached confluent monolayer at day 6 (n ≥ 36).

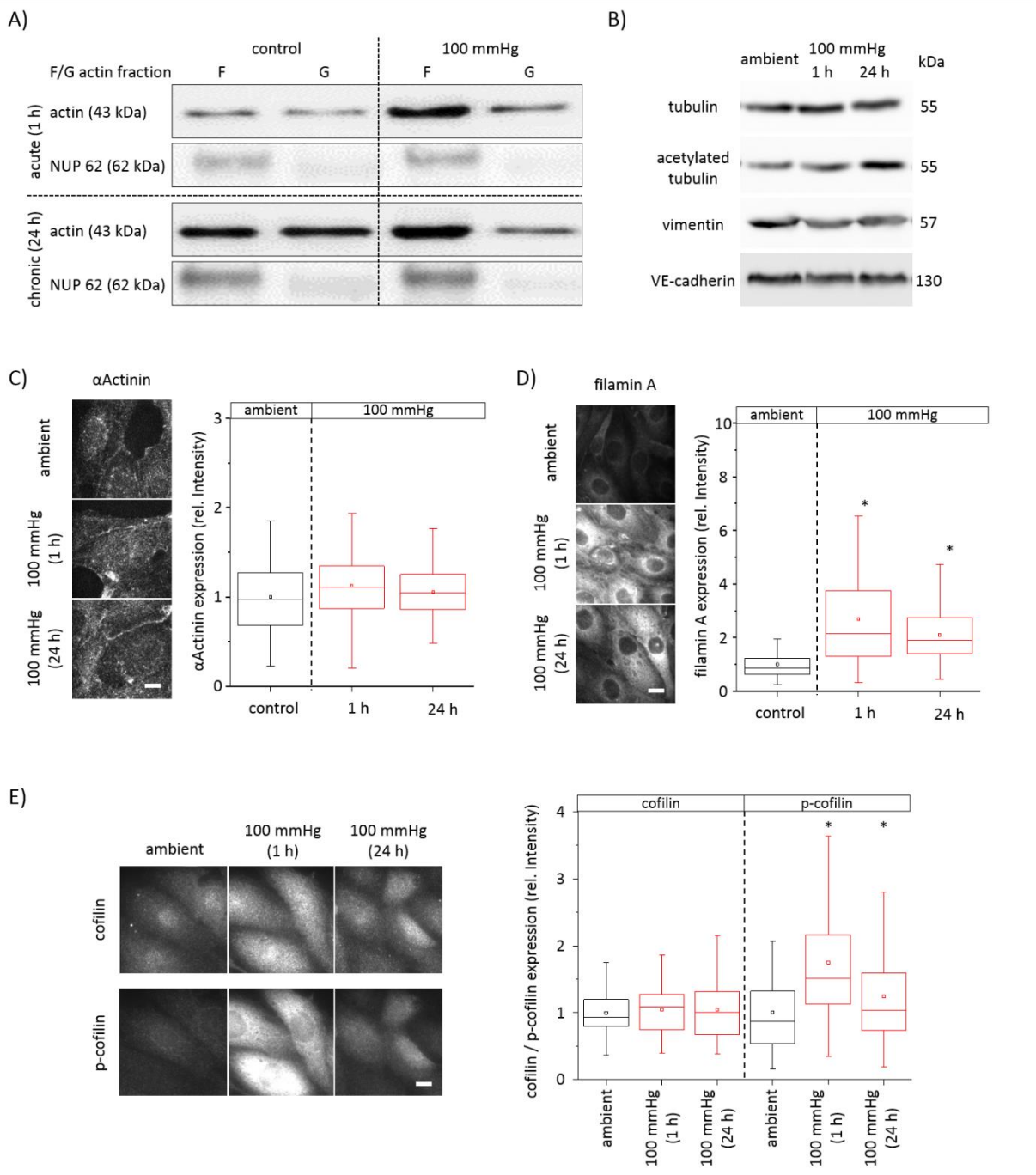

Supplementary figure 2: (A, B) Example western blots of (A) F-/G-actin ratio and (B) detection of tubulin, acetylated tubulin, vimentin and VE-cadherin expression in GM7373 cells. **(C, D, E)** Immunofluorescence staining and quantification of (C) α-actinin (n ≥ 62), (D) α-filamin (n ≥ 98) and (E) cofilin/phospho-cofilin (n ≥ 103) intensities in response to ambient pressure, 1 h or 24 h 100mmHg, respectively. Scale bar = 10 µm. * = significant difference to ambient control.

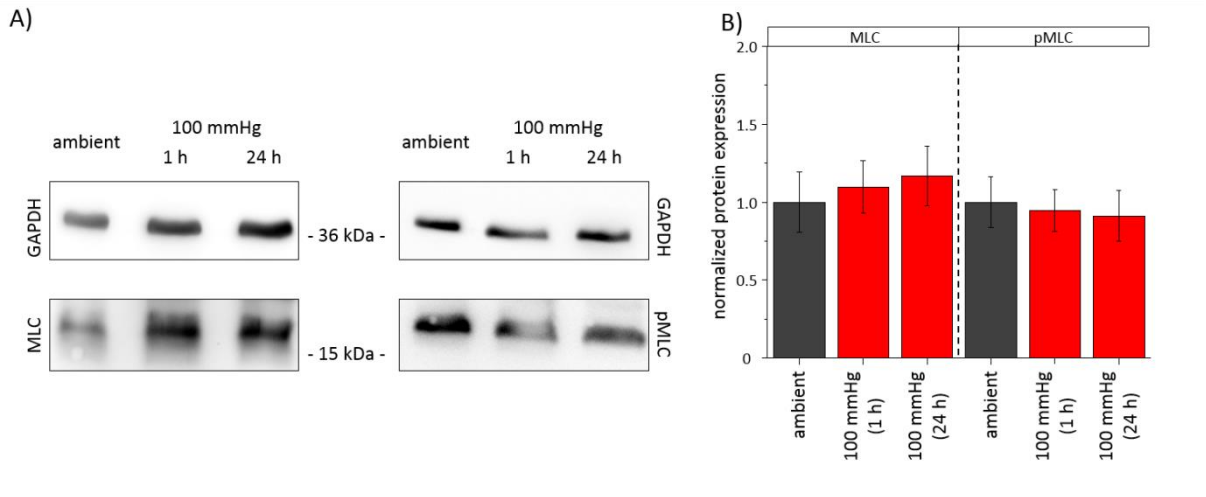

Supplementary figure 3: Pressure-dependent expression non muscle myosin light chain (A) Example Western blot **(B)** and quantification of myosin light chain (MLC) and phosphorylated MLC (pMLC); n =6. * = significant difference to ambient control.

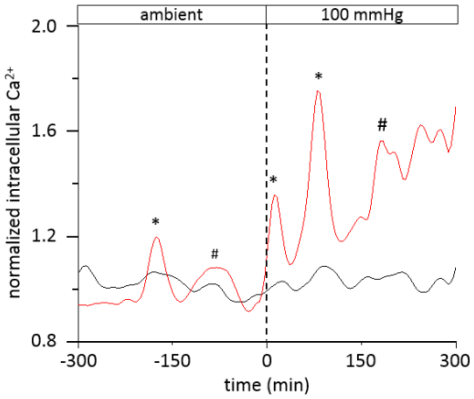

Supplementary figure 4: Example illustrating the distinct populations of endothelial cells with (red) and without (black) intracellular calcium oscillations. * indicate Ca^{2+} peaks used for quantification. # indicates $[Ca^{2+}]_i$ variations below the threshold which were not counted as Ca^{2+} peaks.

A)

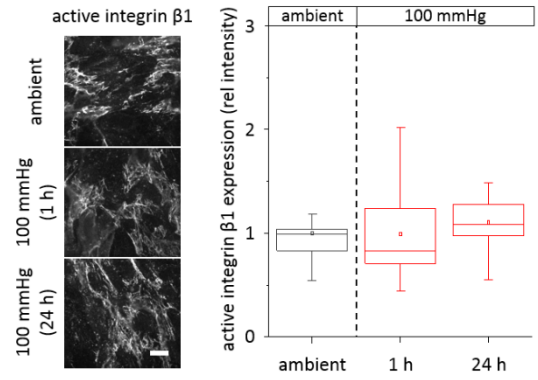

Supplementary figure 5: Immunofluorescence staining and quantification of active integrin β1 (n ≥ 21). No pressure dependent effect was detected. Scale bar = 10 µm

Table S1: gas pressures of media taken from pressure chambers. pH and gas partial pressure measurement verified non-hypoxic conditions in the designed pressure chambers.

		pH	HCO_3^- (mmol/L)	CO_2 (mmHg)	O_2 (mmHg)
acute pressure chamber	HEPES buffer, ambient control (2 h)	7.43	2	3	185
	HEPES buffer, pressure chamber (2 h)	7.43	2	3	193
chronic pressure chamber	medium, cell culture incubator (24 h)	7.45	12	27	187
	medium, pressure chamber (24 h)	7.46	12	22	190

Table S2: **p-values.** Statistical analysis of corresponding figures.

Click here to Download Table S2

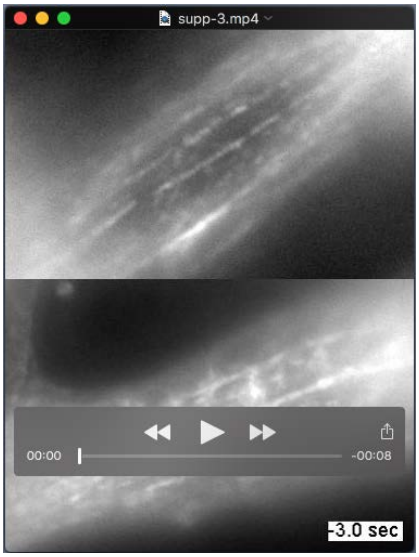

Supplementary movie 1: Single acto-myosin filaments of GM7373 cells expressing MLCb-GFP were cut by laser ablation. Upper panel: example movie at ambient pressure; lower: after 1 h at 100 mmHg.

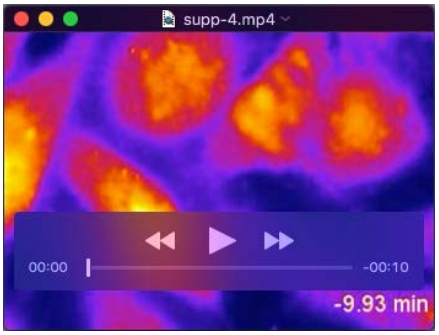

Supplementary movie 2: Intracellular calcium levels in GM7373 cells were imaged by loading with Fluoforte. At time = 0 min pressure was increased from ambient to 100 mmHg. Cycle time 2min.

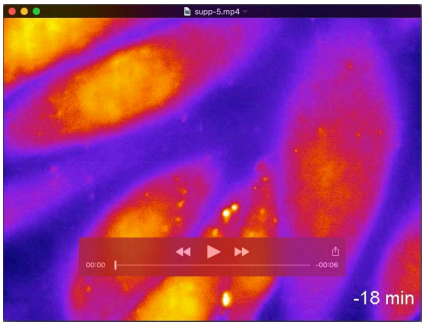

Supplementary movie 3: Intracellular calcium levels in GM7373 cells were imaged by loading with Fluoforte. Due to cycle time of 4 sec, oscillations in intracellular calcium could be observed.